UCRL-53868-00-VOL-1

Engineering Technology Reports Volume I: Laboratory Directed Research and Development FY00

A. L. Baron, R. T. Langland, and C. Minichino

U.S. Department of Energy

Lawrence Livermore National Laboratory

October 3, 2001

This work was performed under the auspices of the U.S. Department of Energy by University of California, Lawrence Livermore National Laboratory under Contract W-7405-Eng-48.

UCRL-53868-00
Volume 1
September
2001

Engineering Technology Reports

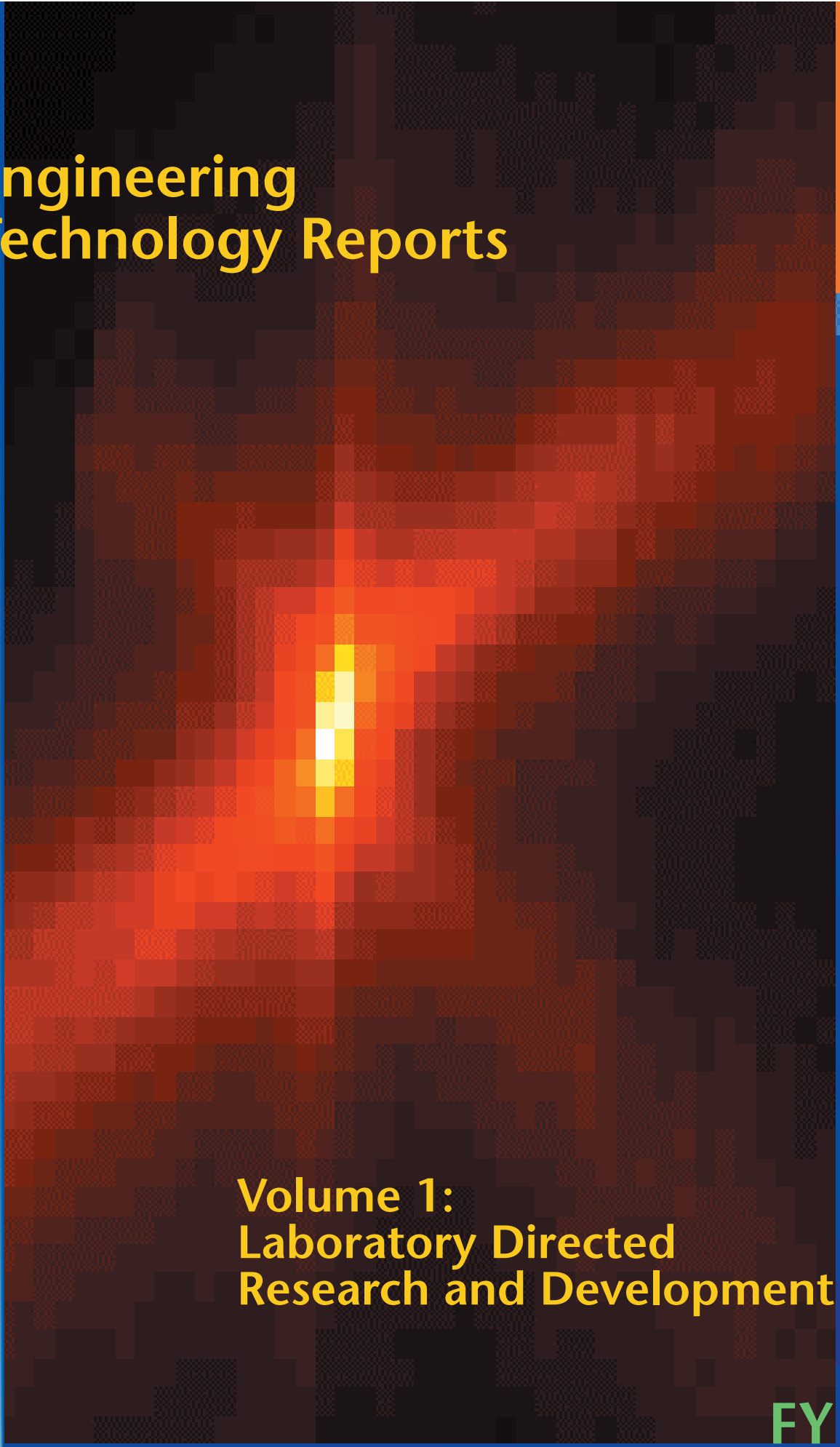

Volume 1: Laboratory Directed Research and Development

FY 00

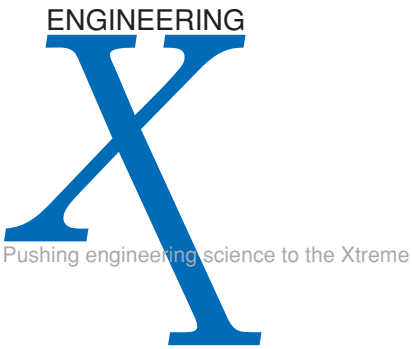

Acknowledgments

Scientific Editing
Andrea L. Baron
Robert T. Langland
Camille Minichino

Graphic Design
Irene J. Chan

Art Production/Layout
Pamela A. Allen
Irene J. Chan
Lucy C. Dobson

Composition
Andrea L. Baron

Document Approval and Report Services
Cynthia Tinoco

Cover:
Stylized graphic of an image from a CCD camera.

UCRL-53868-00
Volume 1
September
2001

Engineering Technology Reports

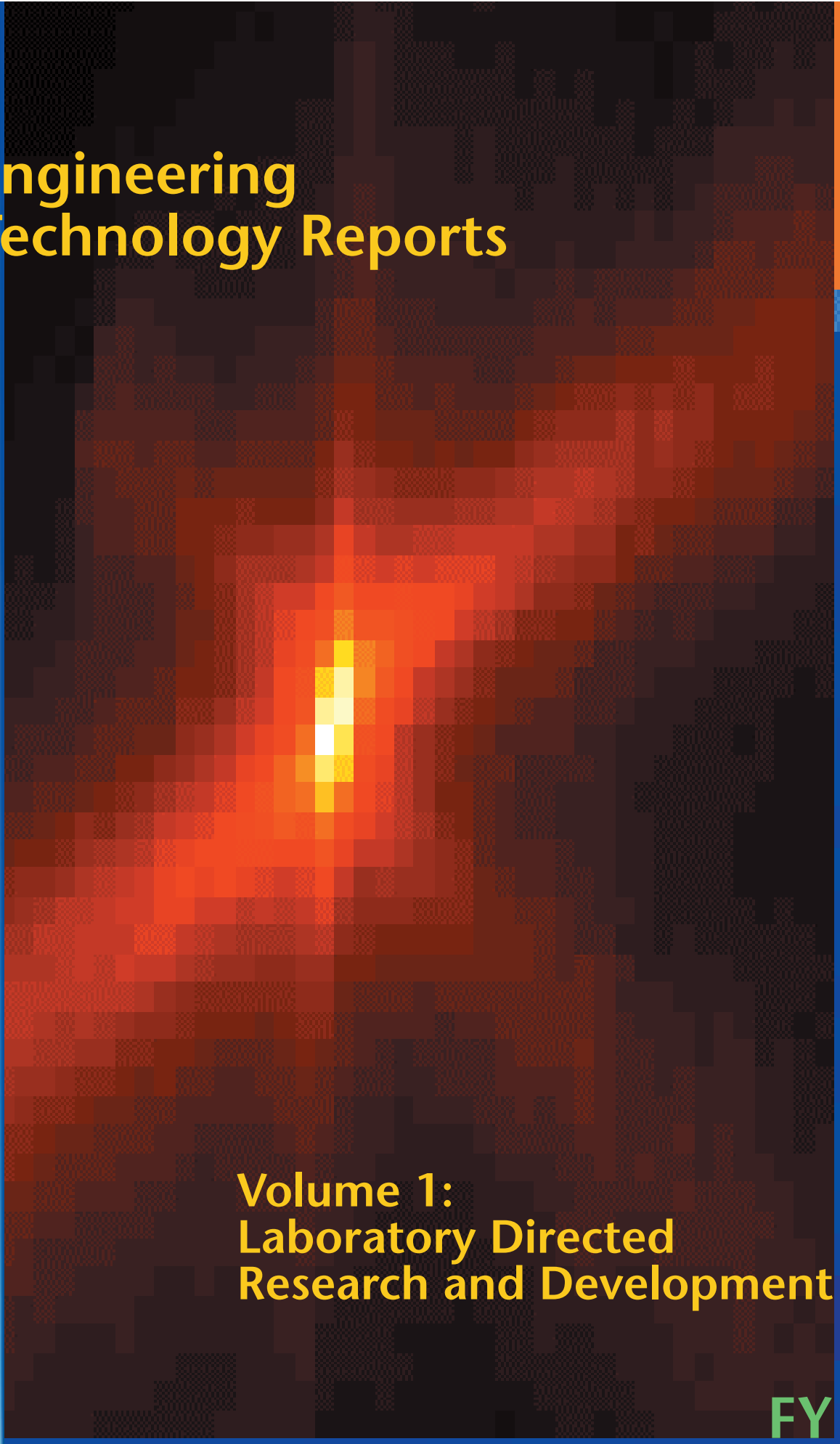

Volume 1: Laboratory Directed Research and Development

FY 00

Introduction

Spiros Dimolitsas, Associate Director for Engineering

600-eV Falcon-Linac Thomson X-Ray Source
J. K. Crane, G. P. Le Sage, T. Ditmire, R. Cross, K. Wharton, K. Moffitt,
T. E. Cowan, G. Hays, V. Tsai, G. Anderson, R. Shuttlesworth, P. Springer 3

RF Photoinjector Development for a Short-Pulse, Hard X-Ray Thomson Scattering Source
G. P. LeSage, S. G. Anderson, T. E. Cowan, J. K. Crane, T. Ditmire, J. B. Rosenzweig 4

Numerical Technology for Large-Scale Computational Electromagnetics
R. M. Sharpe, D. A. White, N. J. Champagne 5

Automated Hexahedral Partitioning of 3-D Space
D. J. Steich, J. S. Kallman 6

Lattice Boltzmann Simulation of Microfluidic Devices
D. S. Clague, E. K. Wheeler, D. Hilken 7

Improved Implicit Finite-Element Dynamics
M. A. Puso, E. Zywicz 8

Quantitative Tomography Simulations and Reconstruction Algorithms
H. E. Martz, Jr., M. B. Aufderheide, III, D. M. Goodman,
A. Schach von Wittenau, C. M. Logan, J. M. Hall, J. A. Jackson, D. M. Slone 9

Photothermal Microscopy: Next Generation Nanoscale Imaging
D. Chinn, C. Stolz, P.-K. Kuo 10

Predicting and Effecting Precise Deformation
D. Swift 11

Updating FEM Using the Extended Kalman Filter and the Gauss-Newton Search
R. R. Leach, Jr., L. Ng, D. B. McCallen 12

A Cooperative Control Architecture for Mobile Robotic Agents
R. Hills, R. S. Roberts, C. T. Cunningham 13

Low-Threshold Oxide-Confined GaInNAs Long-Wavelength Vertical-Cavity Lasers
M. C. Larson, C. W. Coldren, S. G. Spruytte, H. E. Petersen, J. S. Harris 14

LambdaConnect: Multi-Wavelength Technologies for Ultrascale Computing
S. W. Bond, M. D. Pocha, R. R. Patel, E. M. Behymer, G. A. Meyer, P. L. Stephan 15

A MEMS-Based Fuel Cell for Micropower Generation
J. Morse, A. Jankowski 16

Advanced Imaging Catheter
P. Krulevitch, D. Hilken, J.-U. Kluiwstra, R. Miles, D. Schumann, K. Seward 17

Speckle Reduction for LIDAR Using Optical Phase Conjugation
M. Bowers, C. Kecy, L. Little, J. Cooke, J. Bentereau, R. Boyd, T. Birks 18

Dynamic Focusing of Acoustic Energy for Nondestructive Evaluation
J. V. Candy 19

Selected Engineering Publications

Selected Engineering Publications 23

Author Index

Author Index 27

Introduction

Spiros Dimolitsas, Associate Director for Engineering

In FY-2000, Engineering at Lawrence Livermore National Laboratory faced significant pressures to meet critical project milestones, and immediate demands to facilitate the reassignment of employees as the National Ignition Facility (the 600-TW laser facility being designed and built at Livermore, and one of the largest R&D construction projects in the world) was in the process of re-baselining its plan while executing full-speed its technology development efforts. This drive for change occurred as an unprecedented level of management and program changes were occurring within LLNL. I am pleased to report that we met many key milestones and achieved numerous technological breakthroughs.

This report summarizes our technical R&D objectives, methods and key results—as structured through our technology centers.

Whether using computational engineering to predict how giant structures like suspension bridges will respond to massive earthquakes or devising a suitcase-sized microtool to detect chemical and biological agents used by terrorists, we have made solid technical progress.

Five Centers focus and guide longer-term investments within Engineering, as well as impact all of LLNL. Each Center is responsible for the vitality and growth of the core technologies it represents. My goal is that each Center will be recognized on an international scale for solving compelling national problems requiring breakthrough innovation. The Centers and their leaders are as follows:

- Center for Complex Distributed Systems: David B. McCallen
- Center for Computational Engineering: Kyran D. Mish
- Center for Microtechnology: Raymond P. Mariella, Jr.
- Center for Nondestructive Characterization: Harry E. Martz, Jr.
- Center for Precision Engineering: Keith Carlisle

FY-2000 highlights

The **Center for Complex Distributed Systems** exploits emerging information technologies to develop integrated systems for data gathering, processing, and communication, and new methodologies for assimilating measured data with computational models in data-driven simulations. Effective combination of data and simulation leads to enhanced understanding and characterization of complex systems ranging from large applied physics experiments to complex, highly heterogeneous geologic systems associated with underground defense facilities and nuclear materials geologic repositories. The Center's LDRD activities include development of ultra wideband communication technologies for enabling robust and stealthy communications in a cluttered environment, and the development of model-based signal processing algorithms for rigorous updating of finite element models based on measured system response.

The **Center for Computational Engineering** provides for the development and deployment of software tools that aid in the LLNL engineering mission. Highlights of the Center's LDRD projects include 1) A linear-algebra solver effort, among the first in the world to address the full scope of equation-solution efforts in science and engineering. 2) A methodology for handling smooth-surface contact-impact problems in mechanics using faceted low-order approximation technology commonly used in the national laboratory community. This project represents a successful attempt to combine high-order geometric response and low-order approximation. 3) A lattice-based microfluidics simulation tool that permits a wide range of fluid motions to be simulated on parallel computers. This project facilitates the extension of computational fluid mechanics to micro- and nano-technology systems, where the continuum approximations found in classical fluid mechanics no longer apply. Also included is the development of one of the first microfluidics tools capable of using ASCI-class supercomputers.

The mission of the **Center for Microtechnology** is to invent, develop, and apply microtechnologies for LLNL programs in global security, global ecology, and bioscience. Its capabilities cover materials, fabrication, devices, instruments, or systems that require microfabricated components, including microelectromechanical

systems (MEMS), electronics, photonics, microstructures, and microactuators. Center staff have achieved considerable national recognition for the successes demonstrated in Chem-Bio National Security Program instrumentation, supported by the DOE and the Defense Intelligence Agency. Over the last year, nine prototypes of the handheld nucleic acid analyzer, the HANAA, were provided for beta testing by evaluators with a variety of applications, generally focused on bioterrorism response. Work on a microfabricated solid-oxide fuel-cell system, and the Lattice-Boltzmann method for modeling of particles in microfluidics have led to DARPA grants. Work in mesoscale "telerobotic" manipulators has led to a spin-off company.

The **Center for Nondestructive Characterization** advances, develops and applies nondestructive characterization (NDC) measurement science to significantly impact the manner in which LLNL inspects–and, through this, designs and refurbishes systems and components. The Center plays a strategic and vital role in LDRD by researching and developing NDC technologies, such as acoustic, infrared, microwave, ultrasonic, visible and x-ray imaging, to allow future incorporation of these new capabilities in LLNL and DOE programs. The near-term strategic mission objectives are to advance Engineering's core competencies and technologies in quantitative NDC and in fast nanoscale 3-D imaging. This year's LDRD research contributions are in 1) quantitative tomograph simulations and reconstruction algorithms; 2) speckle reduction for LIDAR using optical phase conjugation; and 3) photothermal microscopy: next generation nanoscale imaging.

The **Center for Precision Engineering** is dedicated to the advancement of high accuracy engineering, metrology and manufacturing. The scope of work covers the full range of length scale, from atom-based nanotechnology and advanced lithographic technology to large-scale systems, including optical telescopes and high energy laser systems. A new focus is the manufacturing and characterization of "meso-scale devices" for LLNL's NIF. Millimeter-scale physics experiments will provide data about shock physics, equation of state, opacity, and other essential measurements of weapons physics. One of the highlights of this year's LDRD work is a project to devise and prove a method of dimensional metrology for non-rigid components, *e.g.*, those that can deform during the inspection process. The most noteworthy results are that three dominant FEA uncertainties were identified and quantified, providing a means of improving the credibility of analysis results and also increasing the quantitative usefulness of numerical simulations.

Leveraging our work

In a sense, our Centers serve as the internal venture capitalists for our programs. They provide the mechanism by which Engineering can help LLNL's programs attract funding, while pioneering the technologies that will sustain long-term investment.

Engineering must continually work to build LLNL's competitive advantage; we must continue to create things that are technically one-of-a-kind. Our Centers do this by fusing the best of mechanical and electronics engineering, creating a synergy that most organizations cannot. Our future depends on how we find innovative but cost-effective engineering solutions to emerging technical problems that lead to solutions on a national scale.

LDRD

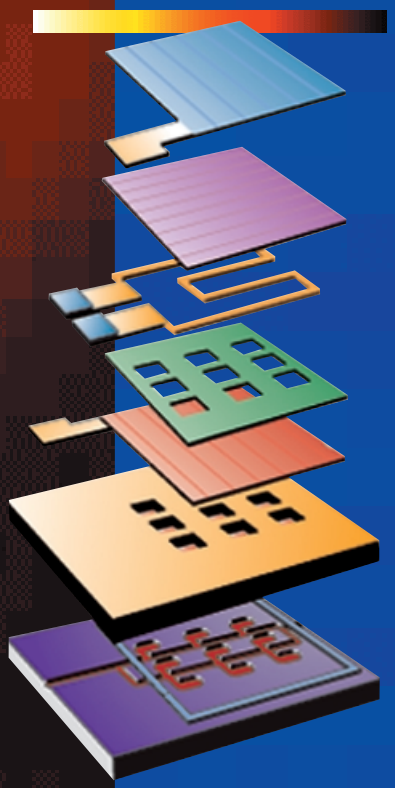

600-eV Falcon-Linac Thomson X-Ray Source

J. K. Crane, G. P. LeSage, T. Ditmire, R. Cross, K. Wharton, K. Moffitt, T. E. Cowan, G. Hays, V. Tsai, G. Anderson, R. Shuttlesworth, P. Springer

There is serious need for an ultrashort-pulse, high-brightness, hard x-ray source capable of probing deep into high-Z solid materials to measure dynamic effects that occur on picosecond time scales. This technique can be used to look at phase transitions, melting and recrystallization, and the propagation of defects and dislocations well below the surface in solid materials, phenomena that are of general interest in solid state physics, materials science, and metallurgy, and have specific relevance to stockpile stewardship.

We have undertaken the development of a Thomson x-ray source, producing x rays by scattering a short-pulse, high-energy laser pulse off a 100-MeV electron bunch from the LLNL linac (Fig. 1). To enable the production of a suitably short pulse of x rays, the linac must be seeded by a short pulse, high-peak-current photoinjector that is synchronized to the Falcon laser system that provides the femtosecond pulse.

In the past year we demonstrated the high-peak-current photoinjector, designed and built the photoinjector laser system (PLS), and synchronized the electron bunch with the Falcon laser system. We plan to upgrade the linac, adding computer controls, and replacing older RF drivers with newer solid-state devices; place the photoinjector on the linac beamline and demonstrate operation of the linac with the photoinjector as the electron seed; and complete the transportation of the full energy beam from the Falcon laser system to the Thomson interaction region.

The PLS, used to generate photoelectrons for the photoinjector, is seeded by stretched pulses from the Falcon laser system so that the linac can be synchronized to the Falcon master oscillator (Fig. 2).

Our ultimate goal is to scatter a 4-J, 100-fs pulse from a 100-MeV, 1-nC electron bunch to produce ~10^9 photons at ~100 keV energy. We have made important progress toward this goal by completing construction and testing of the 5-MeV photoinjector gun and the UV photoinjector laser system. We attempted an experiment to produce and diagnose soft Thomson x rays generated by scattering a weak 800 nm laser pulse from the 5-MeV photoinjector electron bunch. This experiment has given us valuable experience in constructing the interaction chamber, diagnosing spatial and temporal overlap between the electron and laser pulses, and detecting Thomson x rays against a large background of hard x rays produced from the scattered 5-MeV electrons.

In the coming year we will upgrade the Falcon laser system to 10 TW. In the following year we will construct the interaction chamber at the linac output and bring the 10-TW laser pulse to collide with the 100-MeV electron bunch to produce an ultrafast, hard x-ray light source for dynamic, laser-matter interaction experiments at solid densities.

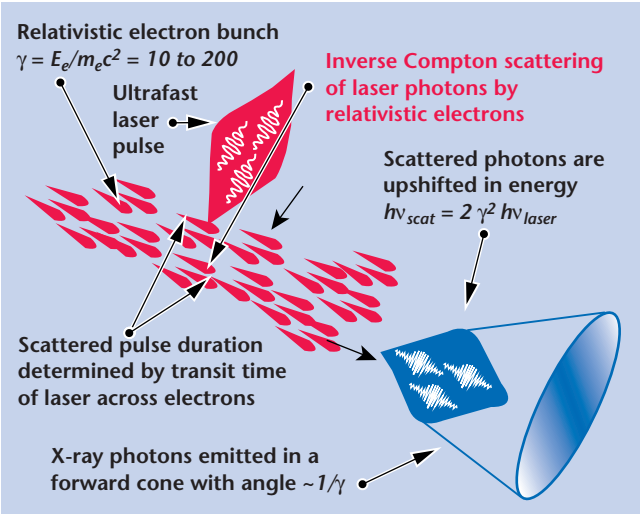

Figure 1. The principle of short-pulse x-ray production via Thomson scattering of visible photons from highly relativistic electrons.

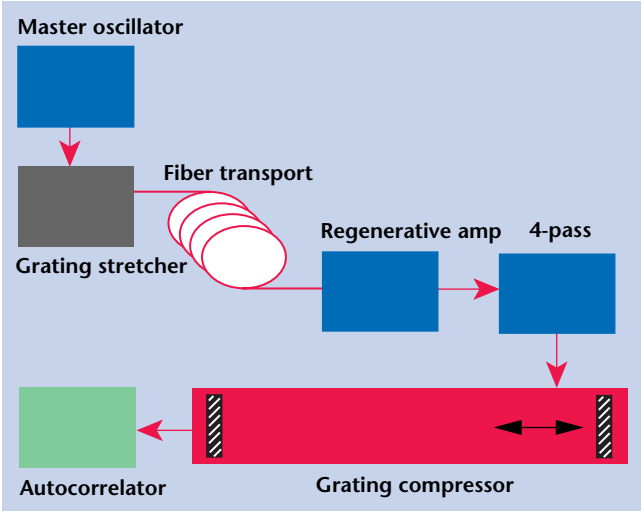

Figure 2. Block layout of the Falcon/Photoinjector laser showing major subsystems.

RF Photoinjector Development for a Short-Pulse, Hard X-Ray Thomson Scattering Source

G. P. Le Sage, S. G. Anderson, T. E. Cowan, J. K. Crane, T. Ditmire, J. B. Rosenzweig

An important motivation in the development of the next generation x-ray light sources is to achieve ps and sub-ps pulses of hard x rays for dynamic studies of a variety of physical, chemical and biological processes. Present hard x-ray sources are either pulse-width or intensity limited, which allows ps-scale temporal resolution only for signal averaging of highly repetitive processes. A much faster and brighter hard x-ray source is being developed at LLNL, based on Thomson scattering of fs-laser pulses by a relativistic electron beam, which will enable x-ray characterization of the transient structure of a sample in a single shot. This source will combine an RF photoinjector with a 100-MeV S-band linac. We have planned a program of beam dynamics and diagnostic experiments in parallel with Thomson source development.

The LLNL Thomson scattering x-ray source combines three subsystems: 1) a 35-fs "FALCON" laser system, currently producing 0.3 J at a 1 Hz repetition rate, with a planned upgrade to 4 J with a 0.1 Hz repetition rate; 2) a photoinjector capable of producing 5-MeV electron pulses with charge up to 1 nC, pulse length of 0.2 to 10 ps, and normalized, rms emittance of 5 π mm-mrad; and 3) an RF linac with output energy adjustable from 30 to 100 MeV. The LLNL system will provide a means of performing pump-probe experiments on a sub-ps time scale, with flux suitable for single-shot measurements. Single-shot measurement enables experiments on samples undergoing irreversible damage: shocks, plasma ablation, or ultrafast melting.

The LLNL photoinjector uses the BNL/SLAC/UCLA 1.6 cell, standing wave accelerator geometry. The photocathode surface has a measured flatness of 79 nm peak-to-valley over a 2-in. diameter (λ/8 at 633 nm). The photoinjector is currently operated separately from the RF linac, and has been fully characterized using a diagnostic beamline. Characterization of the photoinjector has included measurement of cavity Q and filling time, dark current, charge and quantum efficiency, Schottky scan, energy, and emittance. Emittance has also been characterized as a function of charge and pulse length.

The first demonstration of Thomson scattering is planned using the 5-MeV beam directly from the photoinjector interacting with a 30-mJ IR laser pulse produced by the residual energy of the photocathode laser system. The interaction with the 5-MeV beam is expected to produce 10^4 to 10^5 600-eV photons per shot with an interaction angle of 135° between the electron and laser beams. A drawing of the 5-MeV Thomson scattering experiment beamline is shown in the figure.

In addition to the Thomson scattering experiment, the photoinjector and 100-MeV RF linac also provide an ideal test-bed for examining space-charge induced emittance growth effects. A new emittance measurement technique has been demonstrated on the RF linac to characterize the beam produced by the thermionic injector.

The first demonstration of Thomson scattered light from the linac beam and FALCON laser pulses will be the key milestone of the project. After the Thomson scattering demonstration at 600 eV is complete, the next major steps are the installation of the photoinjector on the linac, the propagation of the electron beam through the linac, and the characterization of the 100-MeV beam. Compression of the FALCON beam, and delivery of the laser beam to the linac interaction region will proceed in parallel.

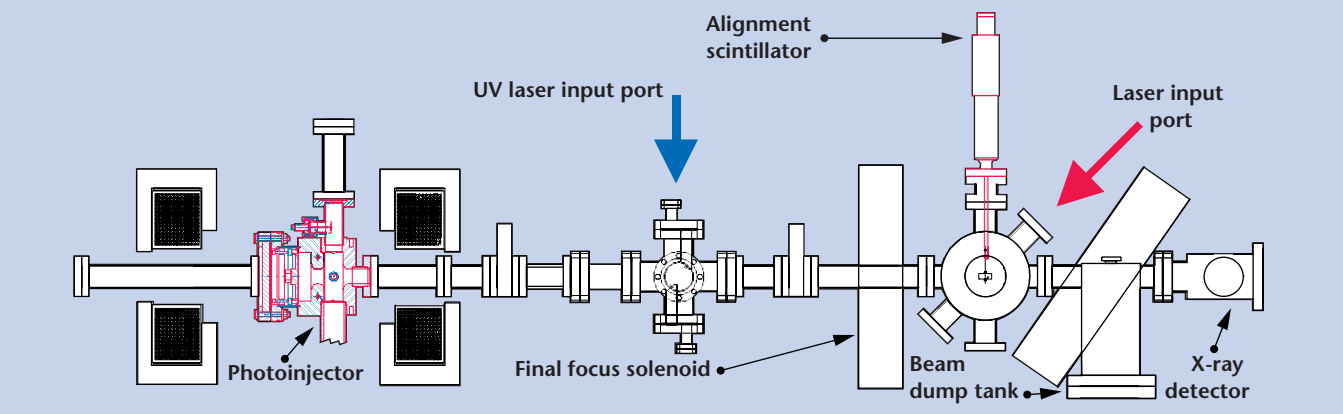

Beamline for Thomson scattering at 5 MeV.

Numerical Technology for Large-Scale Computational Electromagnetics

R. M. Sharpe, D. A. White, N. J. Champagne

The key bottleneck of implicit computational electromagnetics (CEM) tools for large complex geometries is the solution of the resulting linear system of equations. This encompasses virtually all frequency domain solutions of Maxwell's equations. The mathematical operators and numerical formulations used in this arena of CEM yield linear equations that are complex-valued, unstructured, and indefinite. Also, simultaneously applying multiple mathematical formulations to different portions of a complex problem (*hybrid* formulations) results in a mixed-structure linear system (see figure), further increasing the computational difficulty. Direct solution methods, which are currently the state of the art for such hybrid formulations will not scale acceptably for ASCI-class architectures. Approaches that combine domain decomposition (or matrix partitioning) with general purpose iterative methods and special purpose preconditioners are being investigated. Special purpose preconditioners that take advantage of the structure of the matrix will be adapted and developed based on intimate knowledge of the matrix properties.

Initially in FY00, we established a test suite of representative linear systems to provide a test bed for algorithm development and to facilitate collaboration with other research groups. The URL for this effort is http://cce.llnl.gov/solver.

During FY00, we began the development of a solver framework to 1) provide applications with a common interface to a variety of solvers and preconditioners and 2) provide developers with a flexible and extensible system for incorporating new algorithms. Rather than start entirely from scratch, we chose to build upon the ISIS++ Library from Sandia National Laboratories. We re-wrote the ISIS++ software so it could be used for complex-valued linear systems, using generic programming techniques to make the basic abstractions such as vectors, matrices, iterative solvers, and preconditioners independent of data type.

We have generic (type-independent) MPI-based parallel versions of the following Krylov methods: Conjugate Gradient, Conjugate Gradient Squared, Bi-Conjugate Gradient Stabilized, Conjugate Gradient Normal Equations, Conjugate Gradient Normal Residual, Quasi Minimal Residual, Generalized Minimal Residual, and Flexible Generalized Minimal Residual. The modified library is known as ISIS++2.0. This framework is written in the C++ language. To support legacy C and Fortran codes we developed a set of tools that automatically write C and Fortran interfaces to the ISIS++2.0 library. These tools are written in the Perl scripting language. This way, new algorithms can be developed in a modern object-oriented programming language, yet legacy codes can still take advantage of the algorithms. We are in the process of publishing these Perl scripts as an independent by-product of our research efforts.

The next step was to incorporate solution strategies for the hybrid matrices. Initially, our algorithms will be based upon applying the "best" solution procedure to each partition of the overall hybrid system. Using the direct solver, ScaLAPACK, only on the dense partition of the matrix (*e.g.*, Schur Complement method) yields a significant memory savings. For example, for a computer with 8 GB of memory, the direct LU approach restricts us to problems of order 30,000 unknowns, whereas with the Schur Complement approach we can solve systems of order 5,000,000 unknowns.

Even though this is a dramatic memory saving, the ill-conditioning of the overall hybrid systems will require advanced preconditioners to be developed to yield a corresponding reduction in overall solution time. Next year's work will focus on identifying and evaluating advanced preconditioners for the hybrid system and demonstrating the resulting tools on ASCI-class demonstrations.

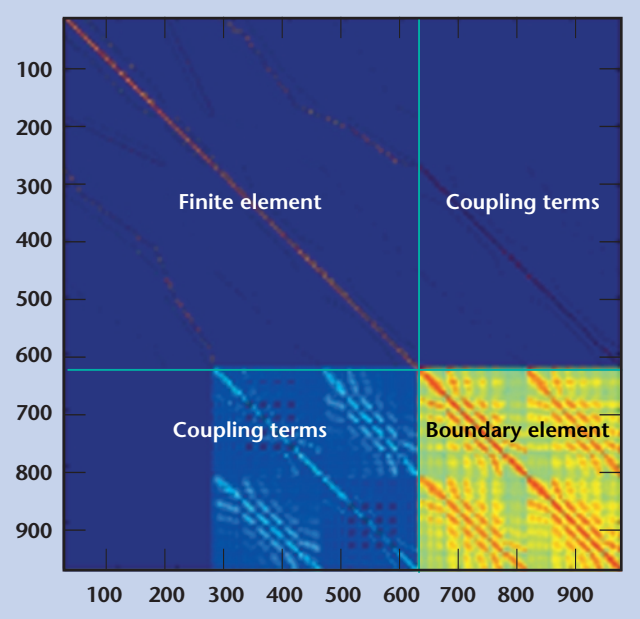

Hybrid matrix example resulting from a coupled finite element / boundary element solution of Maxwell's equations. Blue represents zero matrix values. The finite element (upper left – sparse) represents a discretization of the Helmholtz equation while the boundary element (lower right – dense) represents a discretization of the electric field integral.

Automated Hexahedral Partitioning of 3-D Space

D. J. Steich, J. S. Kallman

Raposdy (Rapid Problem Setup for Mesh-Based Simulation) was a joint LDRD between the Engineering directorate and the Center for Advanced Scientific Computing (CASC). Our project explored automatic partitioning of 3-D space. Once a 3-D space is partitioned into hexahedrals, it is straightforward to obtain a 3-D mesh using transfinite interpolation (TFI) or a similar technique. Currently large amounts of user time are required to generate all-hex meshes using existing software mesh generation packages. The Voronoi tessellation procedure to automate the partitioning of a volume has promise. Considerable progress was made on the problem considering this was just under a one-man-year effort.

Projects like CUBIT are attempting to automate the difficult partitioning process and are proceeding with incremental successes. However, the search for a breakthrough technology to solve the problem continues.

Our accomplishments in FY00 include both 2-D and 3-D explorations of a Voronoi tessellation of space that is subsequently modified to yield an all-hex (or quad) partition of space. The partitioning approach begins with a randomized Voronoi tessellation of space. The resultant mesh at this point is very poor and consists of m-sided, n-faced cells in 3-D, and m-sided polygons in 2-D, with huge edge, area, and volume aspect ratios.

The next step is to successively move each tessellation site to its center of mass and retessellate until convergence is achieved. At this stage, the aspect ratios are much improved but the resulting mesh still consists of m-sided, n-faced cells. The last, most difficult, stage of the automatic partitioning approach is to apply a set of topological changes to the mesh using a threshold annealing optimizer to transform the partitions into all-hexes. A big advantage of the approach is that a valid mesh, which continues to become more hex-centric, is maintained throughout the partitioning process. The disadvantage is that if the optimization procedure gets stuck, the resulting mesh will not be all-hex.

We implemented and tested a full 2-D implementation of the above procedure and were able to automatically partition semi-complex shapes, although the approach was disappointingly CPU-intensive even in 2-D. Numerous variations on the optimization procedure were attempted.

Embedded polygons in arbitrary 2-D shapes posed a difficult challenge for the optimization. The resultant mesh did not always converge to all quadrilaterals. However, the results were encouraging and we began working on a 3-D implementation.

We implemented and tested a 3-D Voronoi tessellation/retessellation procedure as in the 2-D case. The process was very CPU-intensive and required the development of complex oct- and binary-space-partitioning trees along with a vector quantization process to reduce the required CPU loads. We did not pursue the threshold annealing process in 3-D because we wanted the threshold annealing optimization moves to keep faces planar as in the Voronoi process. This constraint limited potential moves available to the annealing process.

We arrived at a way to modify the mesh that in many circumstances immediately yielded an almost all-hex partitioning of the volume. The procedure involved adding nodes to each face and locally cutting each Voronoi cell into a set of local hexahedrals. The procedure we developed is guaranteed to produce an all-hex mesh provided each node of the Voronoi cell is attached to three of the cell's faces, which is often, but not always, the case.

It may be possible to add additional tessellation sites at all nodes, violating the above restriction to guarantee an all-hex mesh in all situations, or to use the threshold annealing process as in 2-D but removing the planarity restriction. These are areas for future research.

Lattice Boltzmann Simulation of Microfluidic Devices

D. S. Clague, E. K. Wheeler, D. Hilken

The design and manufacturing of microfluidics and biological microfabrication and microelectromechanical (Bio-MEMS) devices at LLNL have application to a number of important programs of national interest. For example, biomedical and biotechnology applications include subsystems designed for preparing miniaturized samples and for detecting target species. However, before such devices can achieve desired functionality and ultimately lead to potentially new technologies, many challenging scientific issues must be addressed.

Our project focuses on developing simulation tools to augment and guide microfluidic device designs. Specifically, we are developing lattice Boltzmann (LB) simulation capabilities to study the transport properties of particulate species in microflows. At micrometer-length scales, short-range forces become important. As a result, we are developing simulation capabilities to study coupled physical effects.

During FY00, we focused on the coupling between hydrodynamic and dielectrophoretic (DEP) forces. We performed LB simulations to explore inertial lift effects as a function of Reynolds number, and coupled inertial effects with DEP forces for systems with length scales of actual interest.

Figure 1 shows the extent of lift as a function of Reynolds number; Fig. 2 shows a DEP capture. In Fig. 1, the lift height is made dimensionless with the sphere radius, and the Reynolds number is based on the maximum fluid velocity. According to Saffman's theory (1964), the lift force is proportional to the magnitude of gradient in the velocity profile of the fluid. As the Reynolds number increases, the gradient in the fluid velocity becomes steeper, and the theory predicts an increase in the lift force. Typical Reynolds numbers range from much less than 1 to about 5 in microfluidic systems. As expected, our LB simulations capture the weak inertial forces and predict an increase in lift with an increase in the Reynolds number.

As depicted in Fig. 2, we built a time-averaged electric field into the LB capability to study coupled hydrodynamic and DEP forces on suspended species. As Fig. 2 shows, the sphere initially experiences inertial lift forces; however, when it encounters the electrode array, it is pulled to the electrode surface and captured. Often, device designers want to position target species in the central region of microchannels for detection purposes. Our results in this project now enable the rapid prediction of optimal flow rates for either suppressing or using inertial lift effects to cause the desired repositioning of the particles.

In FY01, we will 1) continue investigating the forces influencing DEP manipulation in flow conditions that are relevant to LLNL's device designers, and 2) explore the inclusion of representative particle geometries in the LB capability. In particular, we will extend our ability to study the transport behavior of macromolecules using ellipsoidal and bead-and-spring models, which are representative of proteins and long-chain polymers (*e.g.*, DNA fragments), respectively.

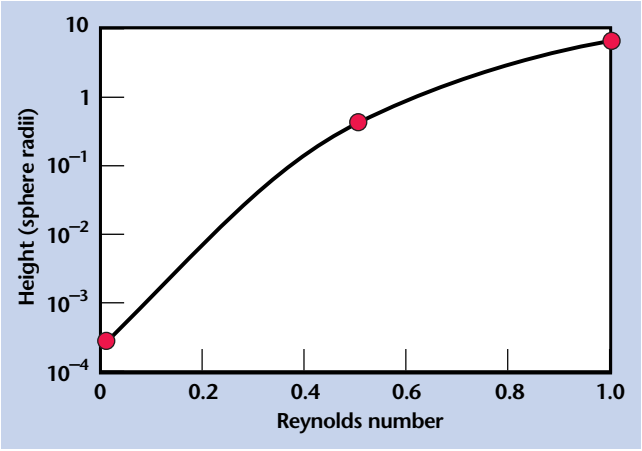

Figure 1. Inertial lift as function of Reynolds number.

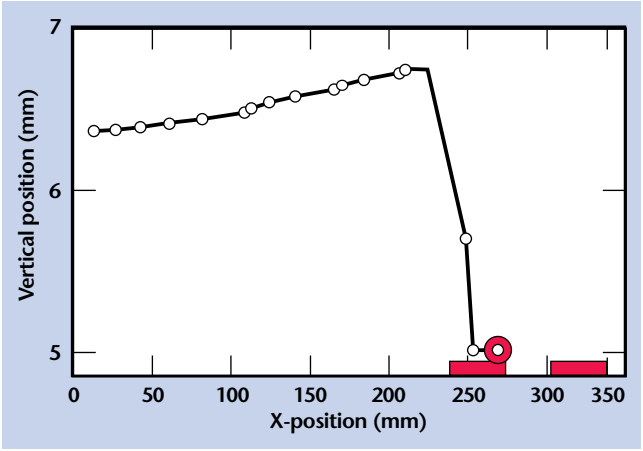

Figure 2. Coupled inertial lift and DEP capture. The rectangles and the sphere represent an electrode array and a target species, respectively.

Improved Implicit Finite-Element Dynamics

M. A. Puso, E. Zywicz

Numerical difficulties encountered with implicit analysis have forced the use of explicit finite-element codes for many problems in mildly nonlinear, static structural mechanics. This is unfortunate, because implicit methods promise better accuracy for nonlinear statics and for long-time, nonlinear dynamics problems such as seismic events, reentry vehicles and transportation container vibrations.

The goal of this project was to develop implicit, finite-element algorithms that solve these problems reliably by attacking the two main obstacles inherent to the implicit method: 1) for nonlinear problems, the classical implicit-integration schemes are numerically unstable, and 2) convergence of the implicit, nonlinear-solution algorithm is severely affected by unilateral constraints on contact surfaces.

During FY00, we developed time-integration schemes that are unconditionally stable for the general setting of coupled (flexible) finite-element and rigid-body analysis. For example, we used a random input to excite a vibration in the FL transportation container shown in Fig. 1. Fig. 2 shows a comparison of the simulated kinetic energy using the old method with that using our new method. Gaps between the foam and cylinder walls cause contact-impact during the motion. With the classical trapezoidal simulation, this contact nonlinearity causes the energy to grow. However, with our new method the energy is controlled. Our work is the first for the general 3-D multibody implicit-dynamics setting and has been the subject of three journal publications.

Contact surfaces are used to interface disjointed objects that impact during analysis. This contact interaction is highly nonlinear and is the major cause of convergence problems. In particular, the non-smooth contact surface causes jumps in contact forces at facet edges and vertices when objects slide past each other. To eliminate this problem, 3-D Gregory patches were used to smoothly interpolate the bilinear surface mesh so that objects will now slide smoothly past each other.

The major technical hurdle overcome in FY00 was the ability to smooth arbitrary, irregular meshes. Smoothing allows the solution to many problems that would have diverged in the past, and is the topic of a recently submitted journal publication.

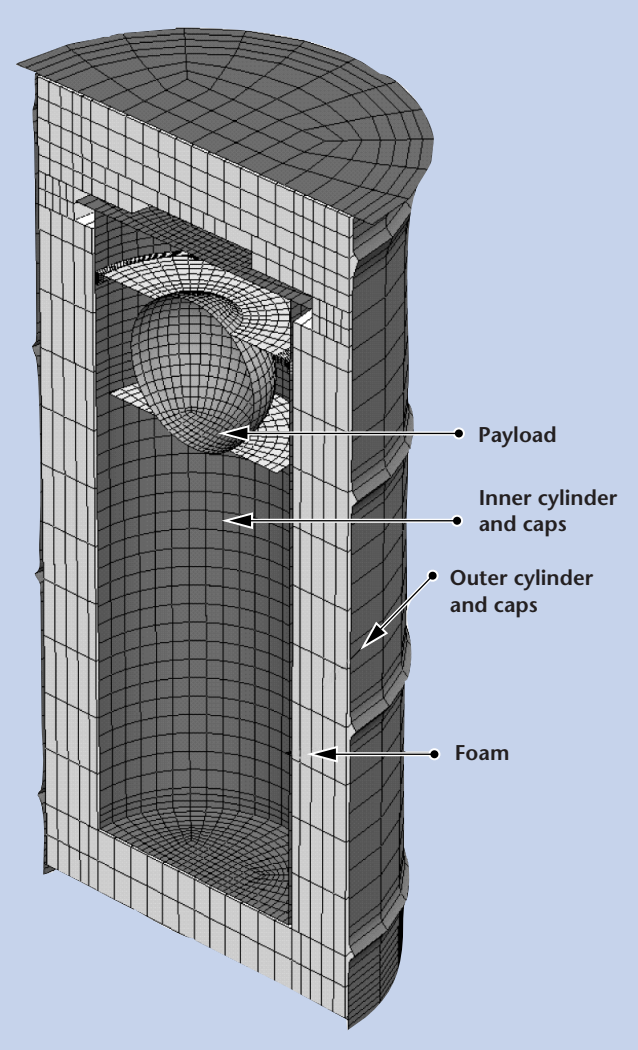

Figure 1. FL transportation container.

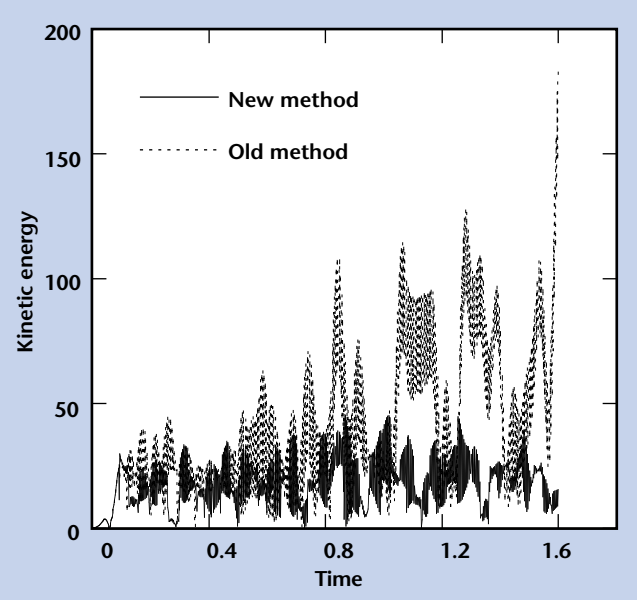

Figure 2. Simulated kinetic energy comparison.

Quantitative Tomography Simulations and Reconstruction Algorithms

H. E. Martz, Jr., M. B. Aufderheide, III, D. M. Goodman, A. Schach von Wittenau, C. M. Logan, J. M. Hall, J. A. Jackson, D. M. Slone

X-ray, neutron and proton transmission radiography and computed tomography (CT) are important diagnostic tools that are at the heart of LLNL's effort to meet the goals of the DOE's Advanced Radiography Campaign. This campaign seeks to improve radiographic simulation and analysis so that radiography can be a useful quantitative diagnostic tool for stockpile stewardship.

Current radiographic accuracy does not allow satisfactory separation of experimental effects from the true features of an object's tomographically reconstructed image. This can lead to difficult and sometimes incorrect interpretation of the results. By improving our ability to simulate the whole radiographic and CT system, it will be possible to examine the contribution of system components to various experimental effects, with the goal of removing or reducing them.

In this project, we are merging this simulation capability with a maximum-likelihood (constrained-conjugate-gradient (CCG)) optimization technique yielding a physics-based, forward-model image-optmization code. In addition, we seek to improve the accuracy of CT from transmission radiographs by studying what physics is needed in the forward model.

During FY00, an improved version of the LLNL ray-tracing code called HADES has been coupled with a recently developed LLNL optimization algorithm known as CCG. The problem of image reconstruction is expressed as a large matrix equation relating a model for the object being reconstructed to its projections (radiographs). Using a CCG search algorithm, a maximum likelihood solution is sought. This search continues until the difference between the input measured radiographs or projections and the simulated or calculated projections is satisfactorily small.

We developed a 2-D HADES-CCG CT code that uses full ray-tracing simulations from HADES as the projector. Often an object has axial symmetry and it is desirable to reconstruct into a 2-D r-z mesh with a limited number of projections. The physics (*e.g.*, scattering and detector response) required in the HADES code is determined from Monte Carlo simulations. The current version of HADES-CCG reconstructs into a volume-density mesh made of one material and assumes a monochromatic source.

Both 10-MeV neutrons and 9-MV x rays were used to image the British Test Object (BTO). This object consists of a set of nested C, W, and polyethylene shells and is used for tomographic algorithm verification. The neutron and x-ray radiographs (figure, left side) of the BTO show some of the joints and different material details. However, it is difficult to use the radiographic projection data to obtain detailed quantitative measurements of features such as joint thickness and material boundaries. To extract more details from the BTO radiographs, a single radiographic projection was used to obtain a 2-D CT cross-section of the BTO (figure, right side). These cross-sections were obtained using the current HADES-CCG code. Comparing the x-ray to the neutron CT reconstructions on the right of the figure, it is apparent that spatial resolution is superior in the x-ray image. This is expected and is largely due to source unsharpness.

Our current implementation of HADES-CCG has shown interesting potential, but more work is needed to make a fully viable reconstruction code. In FY01 we will study the treatment of multiple materials and polychromatic sources in a reconstruction. We will expand the HADES-CCG code to include 3-D reconstructions in FY01, broadening its applicability.

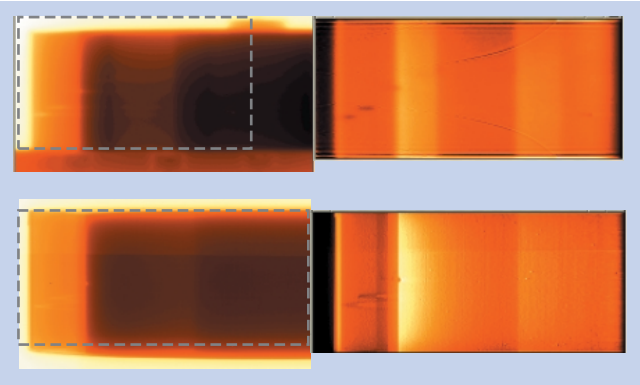

Top left: 10-MeV neutron radiograph of the BTO. Top right: 2-D CT reconstruction of the BTO using the single radiograph shown to the left. Bottom left: 9-MV x-ray radiograph of the BTO. Bottom right: 2-D CT reconstruction of the BTO using the single radiograph shown to the left. The dotted box highlights the portion of the radiograph used to obtain the 2-D cross-sectional CT data in each case. Both CT images were reconstructed into the same voxel size of 0.5 mm x 0.5 mm.

Photothermal Microscopy: Next Generation Nanoscale Imaging

D. Chinn, C. Stolz, P.-K. Kuo

As structures move to smaller scales, higher resolution characterization techniques are needed. Photothermal microscopy (PTM) is a powerful tool for thermal nondestructive characterization of surface and subsurface features with micrometer spatial resolution. PTM offers a higher spatial resolution alternative to infrared imaging. PTM was originally developed as a tool for detecting optical absorption and micrometer-sized thermal inhomogeneities in laser optics. The goal in FY00 was to increase spatial resolution of PTM to 100 nm.

A photothermal tool with nanometer resolution is of great importance in the study of 1) energy deposition and transfer of nanoscale structures such as high-power laser diodes and laser optics; 2) defect detection in coatings such as silicon multilayers; and 3) materials science and manufacturing research. Although the high-power laser projects at LLNL are the direct motivation for this development, applications of this nondestructive characterization tool extend far beyond laser damage to NIF optics. Photothermal and thermo-elastic properties at micrometer and nanometer scale are of great importance to general material science and manufacturing research, for large aperture laser optics as well as nanometer microelectronic devices.

PTM uses scanning pump and probe lasers with a photodetector to measure thermal absorption of materials. The pump laser heats the test object, while the probe laser and photodetector measure the diffraction of light resulting from surface deformation as the heat is absorbed. The spatial resolution of PTM is limited by the pump laser beam size, which can be focused down to the diffraction limit (~1 μm), as described by classical optics.

To increase spatial resolution, implementation of near-field optical techniques to PTM has been investigated. This year, we installed and evaluated a near-field scanning optical microscope (NSOM) for use in nanoscale photothermal experiments. NSOM produces sub-wavelength resolution optical images by scanning an optical fiber over materials. PTM at nanoscale resolution entails using the NSOM fiber probe as the PTM pump laser. An NSOM probe will be used in the PTM pump-probe configuration to achieve nanometer PTM.

We purchased an Aurora NSOM manufactured by ThermoMicroscopes. This NSOM features a scanning stage supported at three points by piezoelectric tubes. The three-point support configuration enables collection of light through a sample in transmission mode. Having access to the sample from beneath the scanning stage is also beneficial for positioning a PTM probe laser.

The Aurora NSOM stage has a tuning fork oscillator attached to the fiber tip that serves as a proximity indicator to sense the distance between the fiber tip and the sample surface. When the tuning fork is driven at its resonant frequency by a lock-in amplifier, the presence of the sample surface within nanometers of the fiber tip increases damping. A feedback loop from the lock-in amplifier controls the vibration of the tuning fork and keeps the fiber tip at a constant distance from the sample.

In evaluating the NSOM, we found that the feedback control system can be further optimized by varying the phase of the lock-in amplifier. Currently, the lock-in amplifier uses the in-phase response. This improvement to the feedback control system will give more precise fiber-part offset distances.

In FY01 we plan to complete the necessary modifications to the NSOM so that nanometer resolution PTM can be tested. Additionally, we will develop a camera-based imaging system that will increase the speed of micrometer resolution PTM.

Predicting and Effecting Precise Deformation

D. Swift

In traditional dimensional inspection, objects are assumed to be essentially rigid. Measurements are taken under a set of constraints that have minimal effect on the overall uncertainty of the measurement. The results, along with a statement of uncertainty, are compared to a design specification. When the object to be measured is not rigid, the contribution of the boundary conditions to the uncertainty in the measurement result becomes significant. Additionally, the dimensional characteristics of the fixtures and supports become confounded with the characteristics of the object being inspected and thus the true shape of the object can not be determined. Finally, if the non-rigid object is put into use under a set of boundary conditions that differ from those present during inspection, the in-use shape is unknown.

Hemi-shells, KDP crystals, EUV Lithography masks, and automobile body parts are all examples where non-rigid components are used under a different set of boundary conditions than those present during inspection. To extend the precision to which these objects can be specified, inspected, and assembled, a new technique in dimensional inspection must be developed and used.

The goal of this project is first to understand methods of restraining or actuating non-rigid objects so that their resulting deformation is repeatable and predictable. While this may appear to be a straightforward analysis problem, it is subject to many sources of error that must be reduced to apply such analysis with high precision. The second goal is to develop a methodology for designing restraints or actuators that produce a predictable deformation on the surface of a non-rigid object and can be modeled analytically with minimum uncertainty. This technique will be applied to a non-rigid cylinder first (see figure) and then extended to include other shapes in the future.

The most noteworthy results from the FY00 effort are that three dominant finite-element analysis uncertainties were identified and quantified. The first was the use of an idealized geometry versus the exact geometry for the analysis. It was found that using the idealized geometry introduced about an 8% error in the result. The second dominant uncertainty was the material properties. We found that uncertainties in the material properties (*e.g.*, elastic modulus, Poisson's ratio, orthotropy) were directly proportional to uncertainties in the analytical result. This uncertainty amounted to about 0.4% in the analytical result. Finally, it was determined that contact at the restraints was difficult to model and characterize and thus contributed to about a 14% error in the result. Because the development of contact algorithms is beyond the scope of the work, we will confine our measurements and analytical comparisons to the regions of the cylinder that are outside the area affected by localized contact.

The FY01 goals of this project are to complete the measurements on the thin cylinder and compare them to the analytical results under various displacement and force boundary conditions. From there, the technique will be extended to a thin hemispherical shell. Additionally, the methodology for designing restraints and actuators will be formalized into a set of design guidelines. These guidelines will serve as the foundation for designing fixtures, mounts, and other constraining devices for non-rigid objects. Finally, a set of metrics will be developed that are function-based rather than geometry-based, to aid in the specification and acceptance of non-rigid objects.

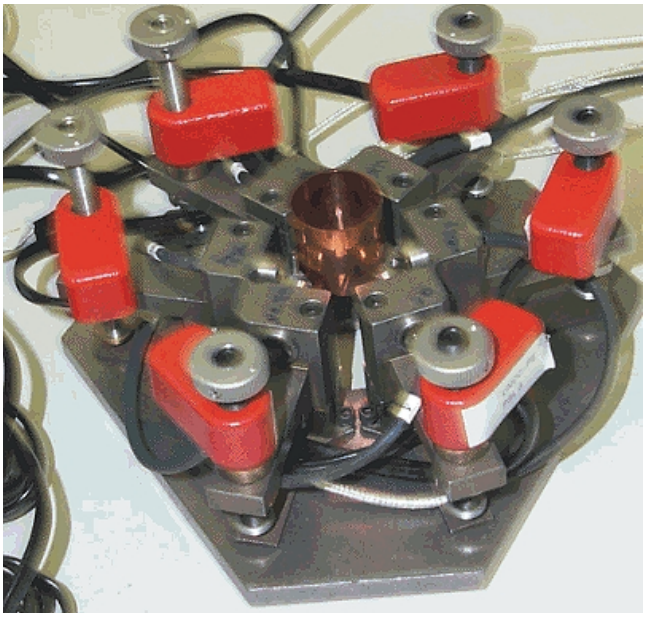

Copper cylinder in measurement fixture.

Updating FEM Using the Extended Kalman Filter and the Gauss-Newton Search

R. R. Leach, Jr., L. Ng, D. B. McCallen

The motivation for this work is to provide a method to update Finite Element Models (FEM) of large structures using state-space-based signal processing techniques. Two different methods, extended Kalman filter, and Gauss-Newton gradient search have been explored. We have made progress in each type of algorithm. We have achieved extremely accurate stiffness, displacement, and velocity estimates for most of the sensor placement scenarios in a five-story building with a simple 10 degrees of freedom (DOF) model.

The primary goal of this project is to develop and apply state-space-based signal processing techniques to locate the existence and type of model mismatches common in FEM.

A simple, 10 DOF FEM of a five-story building is shown in Figure 1. Each floor is represented as a node with mass M, and the nodes are connected by single column elements of stiffness K and damping C. The stiffness elements, K, are estimated by the Kalman filter, the mass and damping values are considered constant. Measurement occurs at the nodes, while the stiffnesses of the columns are the quantities to be identified.

A force was applied to Node M1 consisting of Gaussian noise (0 to 50 Hz). Initial stiffness parameters were set to 7/8, 3/4, 9/10, 1/3, and 1/2 of K, representing a perturbed or "damaged" structure. In the first experiment, the model was fully measured and the stiffness identification errors were essentially zero. Other experiments were then completed (27 total) varying the number of sensors and their locations.

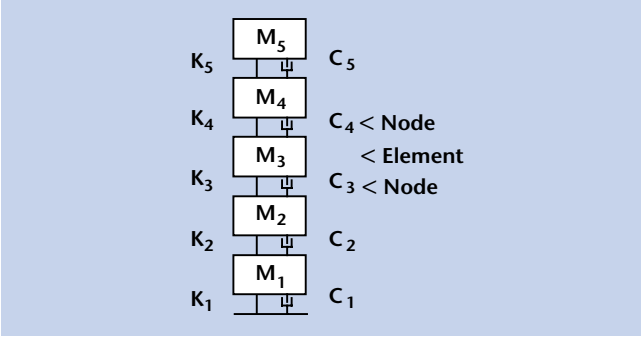

Figure 1. Ten DOF FEM of a five-story building.

The Kalman filter converged very near to the correct stiffness in most experiments with two or more sensors or measurement points. This is particularly promising in that estimates in many cases converged to the correct value even with floors having poorly modeled stiffness parameters. The largest error tended to occur when the uppermost floors were measured (farthest from the vibration source).

The Kalman filter state-space-based parameter identification method works relatively well in this simple 10 DOF identification problem, does not require excessive computational time, and performs consistently for situations where only partial measurement of the system is available.

In the second approach, an iterative Gauss-Newton gradient search routine is used to minimize the residuals in the least squares sense.

Results for both methods are shown in Figure 2. Each column of five boxes represents one unique experiment. The numbers at the top of the boxes corresponds to the average error of the five floors for both the Gauss-Newton method and the Extended Kalman Filter method. A Gaussian noise input was applied to the first floor in all cases.

These results indicate that these methods can be used to update FEMs. They can also be used to identify optimum placement and density of sensors. Finally, we have provided a technique to detect damage in previously tested structures.

This project is completed, allowing us to move toward practical application of this method, *e.g.*, conducting experiments using a shaker table and aluminum tower fixed to the shaker table for controlled testing. There is also potential to extend this work to high-DOF (400 or more) simulated systems.

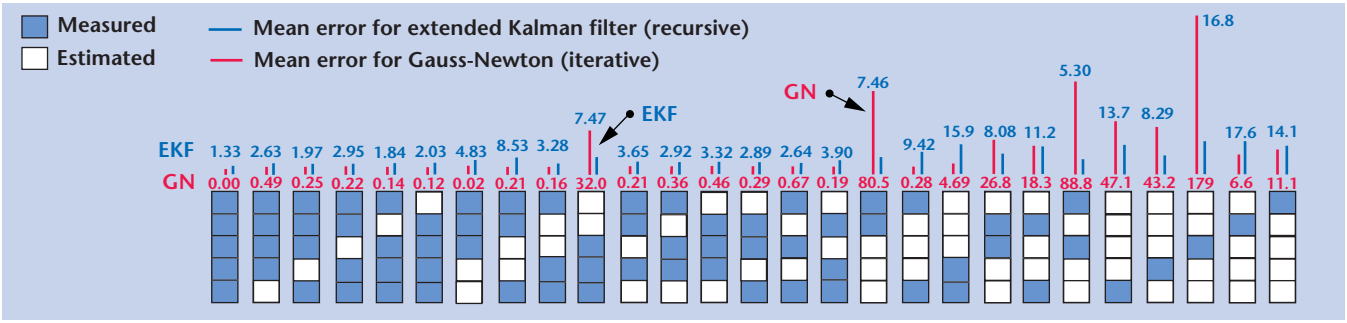

Figure 2. Mean identification error for 5-floor 10-DOF structure using Gauss-Newton method (red bars) and the extended Kalman Filter (blue bars).

A Cooperative Control Architecture for Mobile Robotic Agents

R. Hills, R. S. Roberts, C. T. Cunningham

Large networks of land-based sensors are becoming increasingly important for sensing natural and man-made phenomena. The deployment and operation of large, land-based sensor networks can pose difficult problems, particularly in time-critical situations or in rugged terrains. An example scenario would be one in which ground conditions must be monitored in a forest to enable modeling and predicting the advance of a forest fire. Autonomous deployment and operation of land-based sensor networks in such a scenario are highly desirable for maximizing sensing efficiency while minimizing human risk. Other national security issues involve remote monitoring of sites and facilities (for example, chemical and biological manufacturing facilities), using signatures to determine the manufacturing state of the facilities for counterproliferation operations.

Our approach to the deployment and operation of a land-based sensor network is to use cooperating, unmanned air vehicles (UAVs) that deploy the sensors and then serve as communication hubs for the sensors. In this approach, a group of cooperating UAVs deploys sensors over a region of interest. After the sensors have been deployed, the sensor network is logically partitioned into subnetworks (subnets), with one UAV assigned per subnet. Partitioning the network into subnets allows the UAVs to service sensors in parallel while minimizing interference or duplication of effort. A UAV services the sensors in its subnet by flying a route (path) through the subnet, uplinking data collected by the sensors, and forwarding the data to a central point. Cooperation among UAVs is maintained through the exchange of state information among UAVs, information that includes not only the status of the UAVs but also the status of sensors in the network. In this manner, exceptional events (such as a UAV leaving the network for fuel replenishment or the failure of a group of sensors) can be detected and properly managed by the UAVs.

During FY00, we focused on a key component of the architecture—the adaptive path-planning algorithm. This algorithm initializes the paths and then adapts the subnets (and paths through the subnets) in response to one of four basic exceptions: 1) one UAV leaves the network, 2) one UAV enters the network, 3) several sensors leave the network, and 4) several sensors enter the network. More complex situations can be derived as combinations of these basic exceptions.

The algorithm models the sensor network as a set of directed graphs. In this model, the sensors in a subnet are nodes of a graph, and the UAV path through the subnet is a set of directed links between the nodes. Several approaches have been proposed to find paths through a graph, but these algorithms find the shortest path between two nodes, not a closed path. For the case of one UAV, the problem reduces to the "traveling salesman problem." However, we are interested in applications where multiple UAVs are required to properly service the network.

In the algorithm developed this year, subnet and path adaptation is driven by a global cost function that shifts sensors into and out of subnets to reach a minimum cost. Our heuristic approach—in which we use good approximate solutions and make only minor alterations to them—is quite different from conventional techniques, which consider much more general distortions of existing paths. For example, we found that our method performs significantly better than synthetic-annealing methods used in the past.

In FY01, we will focus on several aspects of the cooperative control architecture, including exception detection, exception handling, and communication networking.

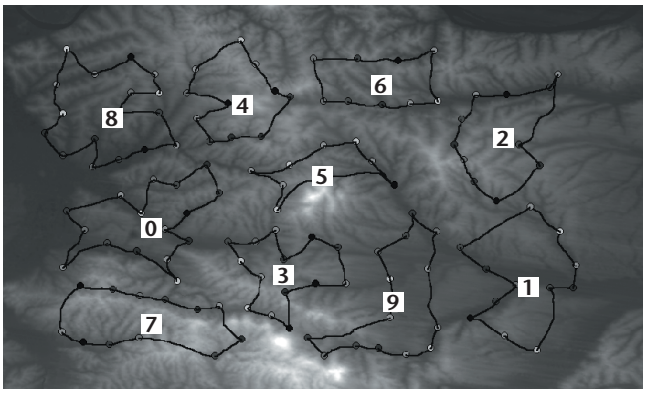

Paths and subnets for the case of 124 sensors and 10 UAVs. The sensor locations were determined using a digital terrain map.

Low-Threshold Oxide-Confined GaInNAs Long-Wavelength Vertical-Cavity Lasers

M. C. Larson, C. W. Coldren, S. G. Spruytte, H. E. Petersen, J. S. Harris

For the first time, we have reported room temperature CW operation of GaInNAs vertical-cavity surface-emitting laser (VCSEL) diodes, emitting at 1200 nm, and grown all-epitaxially in a single step on a GaAs substrate.

Because of its low-cost wafer-scale fabrication and ease of packaging and coupling to optical fiber, the VCSEL (Fig. 1) is an important optical source technology for short-haul optical fiber transmission systems. Dramatic enhancements in bandwidth and distance can be achieved in conventional single- and multimode fiber by extending the VCSEL emission wavelength to the 1300 to 1550 nm range. We have taken advantage of the properties of GaAs-based materials—epitaxially-grown thermally-conductive high-contrast mirrors and AlAs-oxide current apertures—to demonstrate low-threshold VCSELS with CW room temperature operation.

Measurements of the output power and voltage vs. injection current for a device with a 5-μm-x-5-μm aperture show the threshold current at approximately 1.3 mA, and the slope efficiency at 0.045 W/A. An extremely high threshold voltage (10.3 V) resulted from unoptimized doping and composition-grading profiles at the heterointerfaces of the p-DBR (distributed Bragg reflector), creating a large degree of self-heating, which limited the maximum output power to 0.080 mW at 3.8 mA. The fact that CW operation was possible in spite of this excess power dissipation is indicative of the high gain and low temperature sensitivity of the GaInNAs multiple quantum well (MQW) active region.

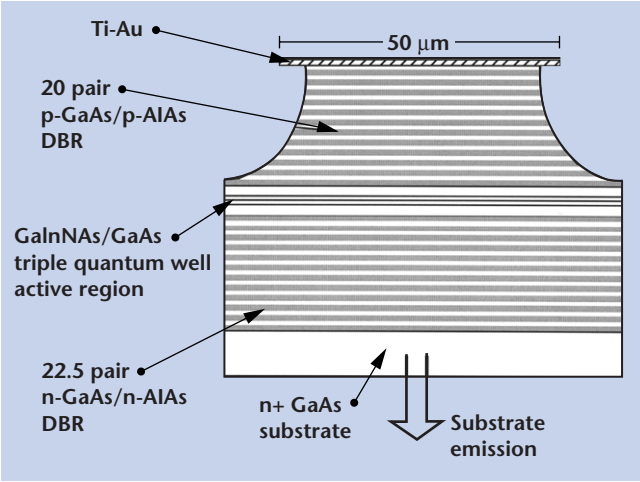

Figure 1. Schematic of GaInNAs VCSEL.

The emission spectrum (Fig. 2) at threshold, indicated that the device lased in a single transverse and longitudinal mode. Above threshold the spectrum exhibited multiple peaks with approximately 0.4-nm spacing and an envelope that broadened with current, which was likely a result of thermally-induced chirp during the current pulse, in conjunction with optical feedback induced by the reflection from the substrate backside.

CW laser operation also occurred for device sizes ranging from 3.6 μm to 6.4 μm, with threshold currents from 0.94 to 2.3 mA and slope efficiency as high as 0.049 W/A.

Devices were also tested under pulsed operation to probe characteristics as a function of aperture size independent of thermal effects. Pulsed threshold current varied from 0.89 mA for 3.6-μm devices, to approximately 21 mA for 29-μm devices. Slope efficiency dropped for aperture sizes below 7 μm, likely due to optical scattering, and current density rose to nearly 7 kA/cm^2 for the smallest devices.

Future improvements in performance should be readily achieved by further adapting well-established 850-nm VCSEL technology. Higher output power will be possible by reducing the resistance of the p-DBR through finer control of composition grading and doping, and lower threshold current by reducing scattering in small-aperture devices. This will also improve high-temperature performance through reduced self-heating. Finally, 1300-nm emission should be achieved by increasing the In and/or N content of the GaInNAs/GaAs MQW active layer.

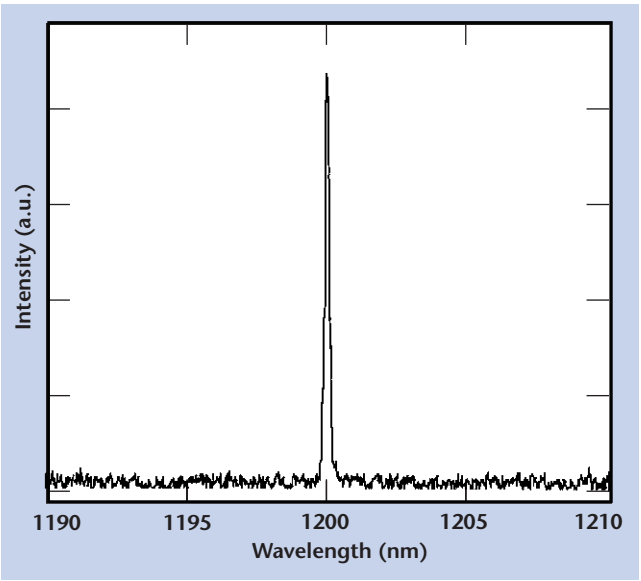

Figure 2. Emission spectrum near lasing threshold.

LambdaConnect: Multi-Wavelength Technologies for Ultrascale Computing

S. W. Bond, M. D. Pocha, R. R. Patel, E. M. Behymer, G. A. Meyer, P. L. Stephan

Ultrascale computing—the integration of large numbers of processors into a single, highly capable multiprocessor system—is currently of great interest for several national security missions. Scalability of these systems, with upwards of hundreds of CPUs, is hampered by the communication bottlenecks imposed by latency, bandwidth, and congestion in electrical interconnection and switching networks. To alleviate these bottlenecks, we are leveraging the recent emergence of low-cost, byte-wide optical components containing linear arrays of multimode optical fibers in ribbon cable assemblies. We have shown that the addition of multiple wavelengths over this byte-wide medium can enable source-routed optical switching, which greatly relieves communication congestion and improves bandwidth.

Implementation of optical source-routed communications fabrics requires the development of novel components, including transmitters capable of fast wavelength tuning and fixed-wavelength optical filters, all compatible with multimode fiber ribbon cables. The system uses an N-x-N optical star coupler as a broadcast element, with the byte-wide wavelength selectable transmitters as inputs, and fixed-wavelength optical receivers as outputs. Switching is achieved by predetermining the output port by appropriate selection of the transmitter wavelength.

This project has focused on the development of prototypes of these components.

We have developed passive alignment techniques using a silicon microbench. Precisely diced VCSEL devices are aligned to multimode fibers using mechanical stops and the ribbon cable alignment pins. We have also investigated post-growth, process tunable VCSELs and multi-cavity filters.

In addition, we have explored the scalability of our system to an ASCI-scale machine, designed for 100 TFLOP/s computation power. An advanced, fully functional LambdaConnect system, with fiber parallelism of 36, and 19 wavelengths per fiber each, operating at 5 Gb/s, functions as a fully non-blocking crossbar switch (no internal contention) with a potential bisection bandwidth of 10.2 Tb/s. Although this is impressive, ASCI performance requirements for balanced computing indicate 1 B of communication for every 10 FLOP, a bisection bandwidth of 80 Tb/s for a 100-TeraFLOP/s system.

We studied the strictly non-blocking five-stage "Clos" switching architecture shown in the figure. The solution we investigated assumed that the 100-TFLOP machine would be assembled from 500 SMP nodes (N = 500), each with 200-GFLOP performance. An optimal solution for a five-stage Clos network with N = 500 has the key solution parameters n_1 = 10, n_2 =5, and r = 10. These parameters were used to calculate the dimensions of the building blocks of the network, to determine the required number of elements per stage, and to estimate the full system cost.

Although we found the cost of an ASCI-scale solution using the Clos network prohibitive, the components and packaging techniques we developed are useful for smaller switching networks and for "fat-pipe" applications, where all wavelengths are used concurrently for byte-wide high bandwidth communication. Potential commercial partners are now reviewing the components and techniques studied throughout this research.

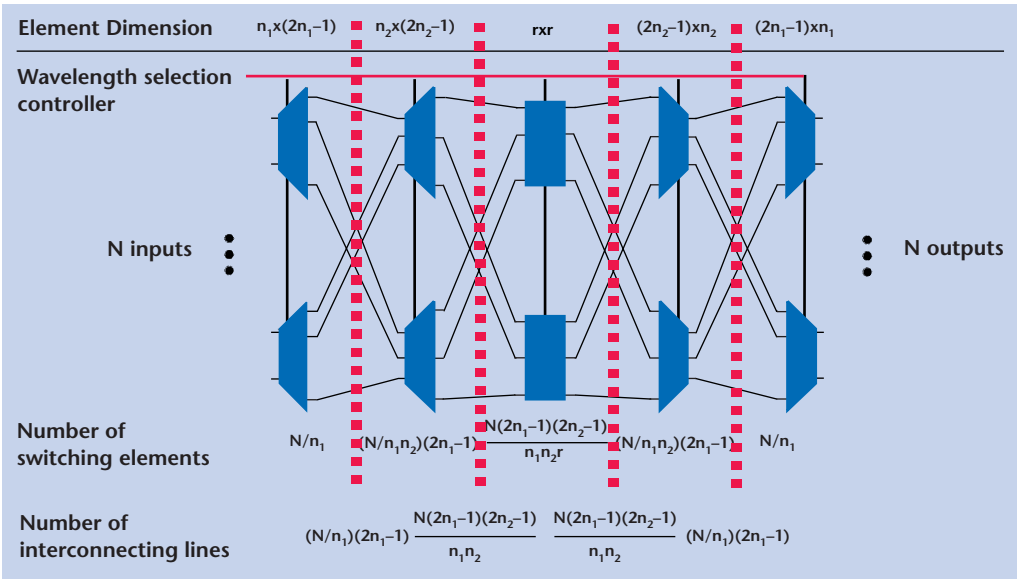

The Clos switching architecture. The interface to each stage of the network (dashed vertical lines) uses an optical-to-electrical and electrical-to-optical conversion, allowing wavelength "re-use" of the coarse wavelength space of LambdaConnect, which is fundamental to allow scaling.

A MEMS-Based Fuel Cell for Micropower Generation

J. Morse, A. Jankowski

New power sources are required for all aspects of the military, weapons testing, and intelligence community, with many of these having specific performance criteria for the direct application. A light-weight, long-lasting power source provides new functionality to missions of all kinds, promising long-term cost benefits to all government agencies, enabling new levels of safety and security for personnel in the field, along with general national security.

The goal of this project is to create a working integrated MEMS-based (combining micromachining, microfabrication, and thin film technologies) fuel cell that delivers power in the 0.5 to 3.0 W range. This power source will exhibit longer mission durations than existing battery technologies, and be designed for specific implementation in wireless remote sensing applications.

We will further incorporate a microfluidic catalytic fuel processor with the fuel cell to reform hydrocarbon-based fuels having high specific energy content, thereby providing an integrated power solution targeting the 0.5 to 20 W range. Through the combination of thin films materials, microfabrication, and silicon micromachining at LLNL, a materials and fuel flexible power source is realized, as illustrated in the figure.

This represents a completely new approach to fuel cell technologies, and opens a new range of applications for fuel cells providing power for autonomous sensor networks being developed for national security requirements. The MEMS-based fuel cell offers advantages in terms of manufacturability, fuel flexibility, reduced temperature of operation, and higher specific energy in comparison to other fuel cell and battery technologies. A further advantage is the direct scalability of this approach through stacking of individual fuel cell modules, achieved through micromachined packaging methods. This enables a wide range of power requirements to be addressed with a common module design.

Results to date have demonstrated the lowest temperature of operation anywhere of a solid oxide fuel cell, exhibiting very competitive power densities for both solid oxide and proton conducting electrolyte materials. Having made these key demonstrations, present efforts are directed towards increasing the power output density of the thin film fuel cells. We have done this by extending the total surface area to which fuel is manifolded through novel integration processes that produce porous host/manifold structures and electrodes, thereby enabling an atmospheric pressure, air breathing fuel cell device.

Efforts during FY00 have continued to optimize the process integration of the electrode/electrolyte material and structure for both PEM and solid oxide fuel cells. Gas diffusion electrode support structures fabricated in silicon substrates using deep anisotropic etch techniques will enable a highly porous host structure for gas diffusion to the anode. At the same time they will retain the necessary mechanical strength to withstand high temperature swings and pressure gradients.

Subsequently, thin film anode-electrolyte-cathode layers are deposited on the gas diffusion electrode supports to form the actual fuel cell structure. At this stage the cells are ready for test. High temperature package and fixturing are presently being designed and developed.

The next phase of this work is to form complete packaged systems for the MEMS-based fuel cells. Subsequent design and testing will explore integrated heaters, and direct use of methanol fuel.

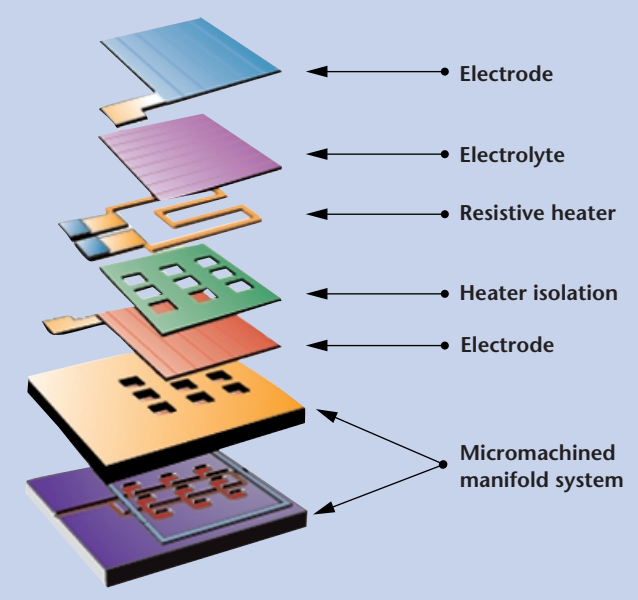

Schematic illustration of MEMS-based fuel cell concept.

Advanced Imaging Catheter

P. Krulevitch, D. Hilken, J.-U. Kluiwstra, R. Miles, D. Schumann, K. Seward

Catheter-based, minimally invasive surgery is performed by making a small incision in a main artery, inserting a long, hollow tube (catheter), and navigating through the artery to the treatment area. Once positioned, the catheter is used to deliver devices such as angioplasty balloons and stents for opening occluded arteries. Over 700,000 catheter procedures are performed annually, and the advantages of this technique—reduced patient trauma and fast recovery—make it one of the fastest-growing surgical procedures. In most cases, catheters are positioned using radiography for visualization, and manual manipulation for navigation and positioning of the device. We are addressing the difficulties associated with current procedures.

The objective of this project is to enhance the physician's navigational abilities by producing a compact catheter that offers imaging and active control to guide and position the distal end (the end inside the body). Clinicians have emphasized that such a device would be a tremendous breakthrough. In addition, this technology has the potential for noninvasive or minimally invasive imaging of explosives or weapons systems.

Over the past three years, we have applied LLNL's expertise in optical and ultrasonic imaging, microfabrication, and modeling toward the development of an advanced catheter. The emphasis for FY00 was on catheter articulation, mesoscale polymer molding and extrusion, and forward-looking ultrasound. In collaboration with physicians at the University of California, San Francisco and the University of California, Davis, we observed several catheter-based procedures and discussed how an articulating, imaging catheter could improve their patients' outcomes. Prototype devices incorporating shape-memory alloy (SMA), shape-memory polymer (SMP), and hydraulic actuation were fabricated and tested. The figure shows an SMP catheter tip with an embedded SMA spring. Heating the composite device just above the SMP transformation temperature causes it to expand and lengthen; heating above the SMA transformation temperature causes it to contract, enabling advancement of the tip when combined in series and actuated peristaltically. By fabricating and testing a 1-in.-long, 0.16-in. inside diameter 0.08-in. outside diameter, hydraulically actuated, molded silicone catheter tip, we demonstrated repeatable 90° bending. In addition, a fluid-filled, 0.25-inch-diameter polymer bellows was shown to increase in length 0.5 in. when heated by a laser.

During FY00, we also investigated using forward-looking ultrasound to aid in guiding a needle during an intravascular liver-bypass procedure known as transjugular intrahepatic portosystemic shunting. In this procedure, a single-element piezoelectric transducer is placed at the end of the articulating catheter and periodically pulsed. Harder tissues reflect more acoustic energy compared to blood-filled veins, thus enabling navigation through a diseased liver. To demonstrate the principle, we placed a single-element, circular transducer in a water bath 40 mm from a vessel-mimicking tube. The first interface was the front wall of the tube, and a large amount of energy was reflected back to the transducer. A second, much smaller reflection was observed coming from the back wall of the tube. This demonstrates the ability to use ultrasound to measure both the distance to the vessel and the size of the vessel. Numerical simulations optimized the size and shape of the transducer.

Several patents have been filed from this project, and two have been issued.

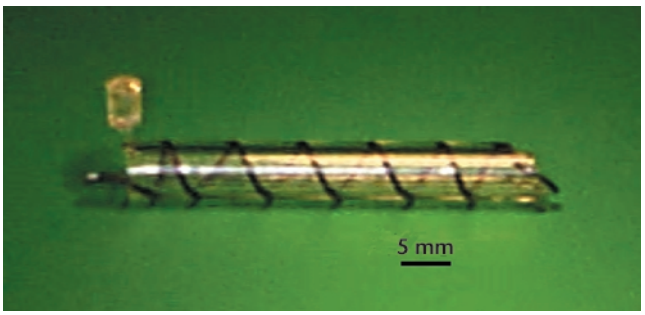

Our advanced, composite catheter tip, showing a prototype shape-memory polymer tip with an embedded shape-memory alloy spring.

Speckle Reduction for LIDAR Using Optical Phase Conjugation

M. Bowers, C. Kecy, L. Little, J. Cooke, J. Bentereau, R. Boyd, T. Birks

Remote detection of chemicals with LIDAR (Light Detection and Ranging) using DIAL (Differential Absorption LIDAR) is now a standard detection technique for both military and civilian activities. We have developed a novel nonlinear optical phase conjugation system that can reduce the effects of speckle noise and atmospheric turbulence on DIAL remote detection systems. We have shown numerically and experimentally that it is possible to increase the signal-to-noise (S/N) ratio for LIDAR systems under certain conditions using optical phase conjugation. This increase in S/N can result in more accurate detection of chemical effluents while simultaneously reducing the time necessary to acquire this information.

A LIDAR system is one in which a laser beam is transmitted out toward an area to be probed. The return scatter from the aerosol itself or the topographic background is detected and measured. In the DIAL technique two or more laser pulses of different frequencies are transmitted sequentially toward a target area. The differences in return signal power for each of these frequencies is measured. Since it is assumed that the returned power would be identical for all frequencies in the absence of absorption, this differencing technique can determine the relative absorption at the transmitted frequencies.

In practical, field operational systems, this simplistic view is complicated by noise sources, such as speckle, which results from the light scattering off a diffuse surface, resulting in a random, but deterministic, light irradiance at each point in the detector aperture.

Optical phase conjugation is a nonlinear optical method of removing the phase differences of the diffuse rays of light. Thus, light can be made to sum constructively over the entire detector aperture, removing the presence of a speckle pattern and the associated noise. DIAL systems require optical pulses of several hundred microjoules or more over many tens of nanoseconds. Because of this, and the high-spatial-frequency content of the DIAL return signal beam, stimulated Brillouin scattering (SBS) was selected as the phase-conjugation method.

For SBS to compensate for the speckle, the optical beam must pass twice through the distorting regions (see figure).

During the course of this project we were able to show that optical phase conjugation can, under certain conditions, improve the S/N of DIAL LIDAR signals. We were able to demonstrate this in the lab as well in computer simulations. We were able to phase conjugate 1530-nm light in optical fibers, for what we believe to be the first time anyone has done this with ns-scale pulses. We also demonstrated the large numerical aperture fibers with appropriate tapers necessary for the optical phase conjugation system to be compact and yet still acquire the DIAL signal.

However, due to the problems with the sapphire fiber crystalline structure and the low numerical aperture of the silica fibers, we were not able to demonstrate this system at the 1-km distances that we had anticipated. We do believe, however, that we have paved the way for this technology to be successful in the near future. We are planning to expand the scope of the work to find appropriate fibers that will facilitate the transfer of this technology to DIAL LIDAR systems in the field.

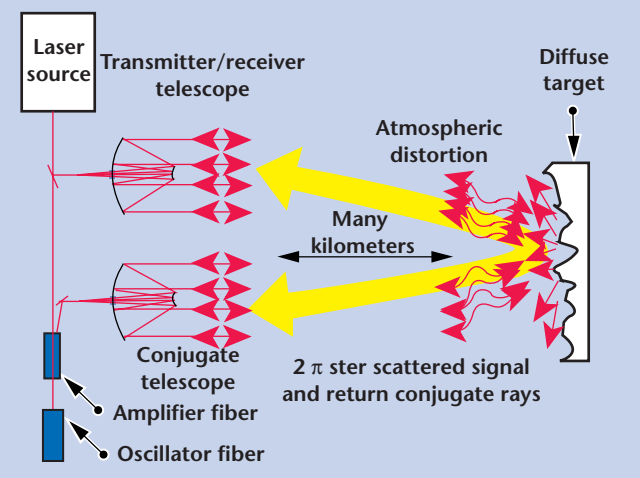

The two-round-trip optical phase conjugation system. The initial probe beam is reflected into 2 π ster. A second telescope captures part of this beam, attenuating it 80 to 100 dB. The beam is transformed into pulse format by a BEFWM process, timed appropriately for SBS amplification. The next time the now pulsed conjugate signal beam is transmitted back to the target, a much larger fraction of the light will return to the original transmitting telescope than would be expected from linear light propagation. This is due to the phase conjugate properties of the light. The light can now be detected with little or no speckle noise.

Dynamic Focusing of Acoustic Energy for Nondestructive Evaluation

J. V. Candy

The inspection of parts, whether lenses for optical systems or components of sensitive weapons systems, must be accomplished as part of a regularly scheduled maintenance and monitoring program, especially during the assembly process. The impact of this project will be considerable for inspecting optics at the National Ignition Facility, and component parts for stockpile stewardship, for noninvasive treatments in the medical area, and for underground target location.

This project is concerned with the R&D required for a technique to dynamically focus acoustic energy for both detection and characterization of flaws for the nondestructive evaluation (NDE) of parts under ultrasonic testing. We have proposed a systematic approach incorporating detailed simulations, algorithm development, hardware, proof-of-principle NDE experiments and prototype design of a viable flaw detection/localization/imaging system.

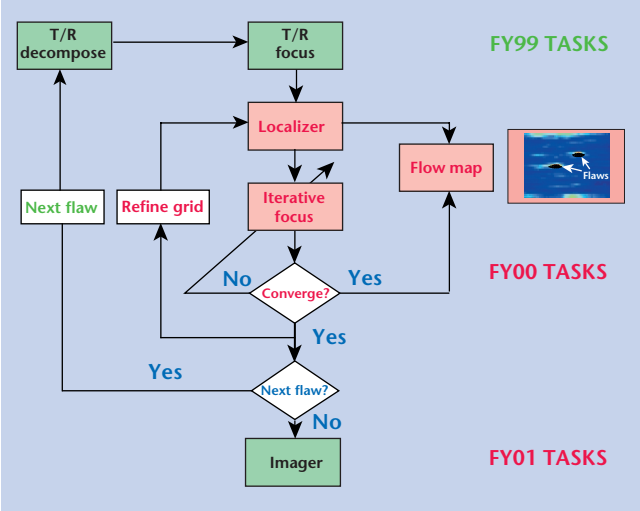

Figure 1. Flaw localization and mapping algorithm.

Dynamic focusing is based on the concept of time-reversal (T/R). T/R processing of noisy ultrasonic sensor array measurements is a technique for focusing energy in various media. The T/R processor can effectively be used to detect flaws (or scatterers) by using its primary attribute—the ability to iteratively focus on the strongest flaw. A T/R processor simply receives the multichannel time series radiated from the region under investigation, collects the array data, digitizes, *time-reverses* the sensor array signals and re-transmits them through the medium to focus.

Using T/R, we have developed algorithms to iteratively decompose the received field into its constituent scatterers, even when they overlap temporally. The overall structure of the approach is shown in Fig. 1. Typical results are shown in Fig. 2 for a homogeneous aluminum part with flaws.

During FY00 we have developed temporal techniques that exploit the T/R focusing property and constructed new processing algorithms.

In FY01, we plan to continue the theoretical investigation of the T/R operator and time domain decomposition algorithms, investigate imaging techniques using the estimated number and location of the flaws, complete the development of a prototype system, and perform proof-of-principle NDE experiments on materials and parts of interest to LLNL.

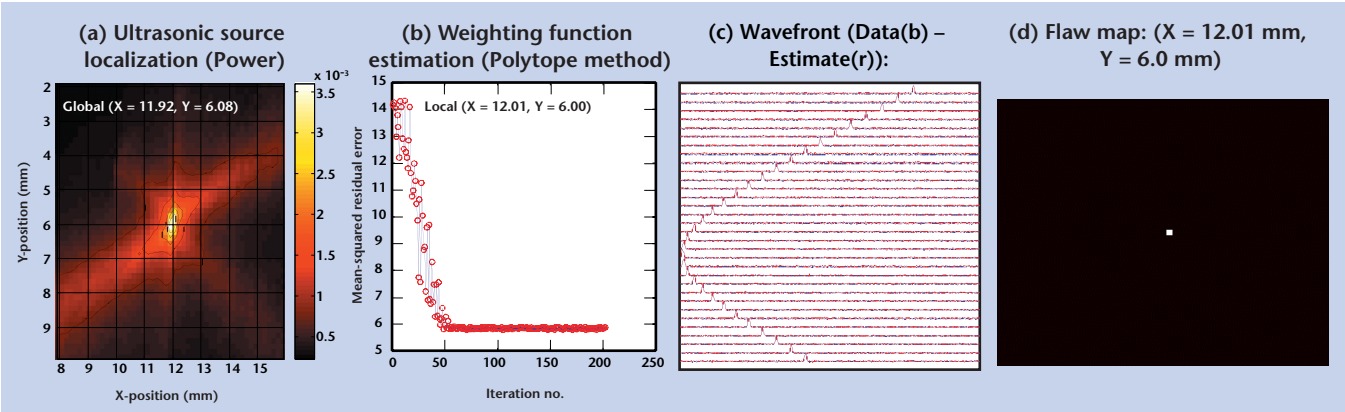

Figure 2. Application of flaw localization and mapping algorithms using T/R processing. Shown are (a) global (ultrasonic source localization), and (b) local (weighting-function estimation) search results for a synthesized aluminum slab. The wavefront match (c) and the final flaw map for a single flaw (d) are also shown.

Selected Engineering Publications

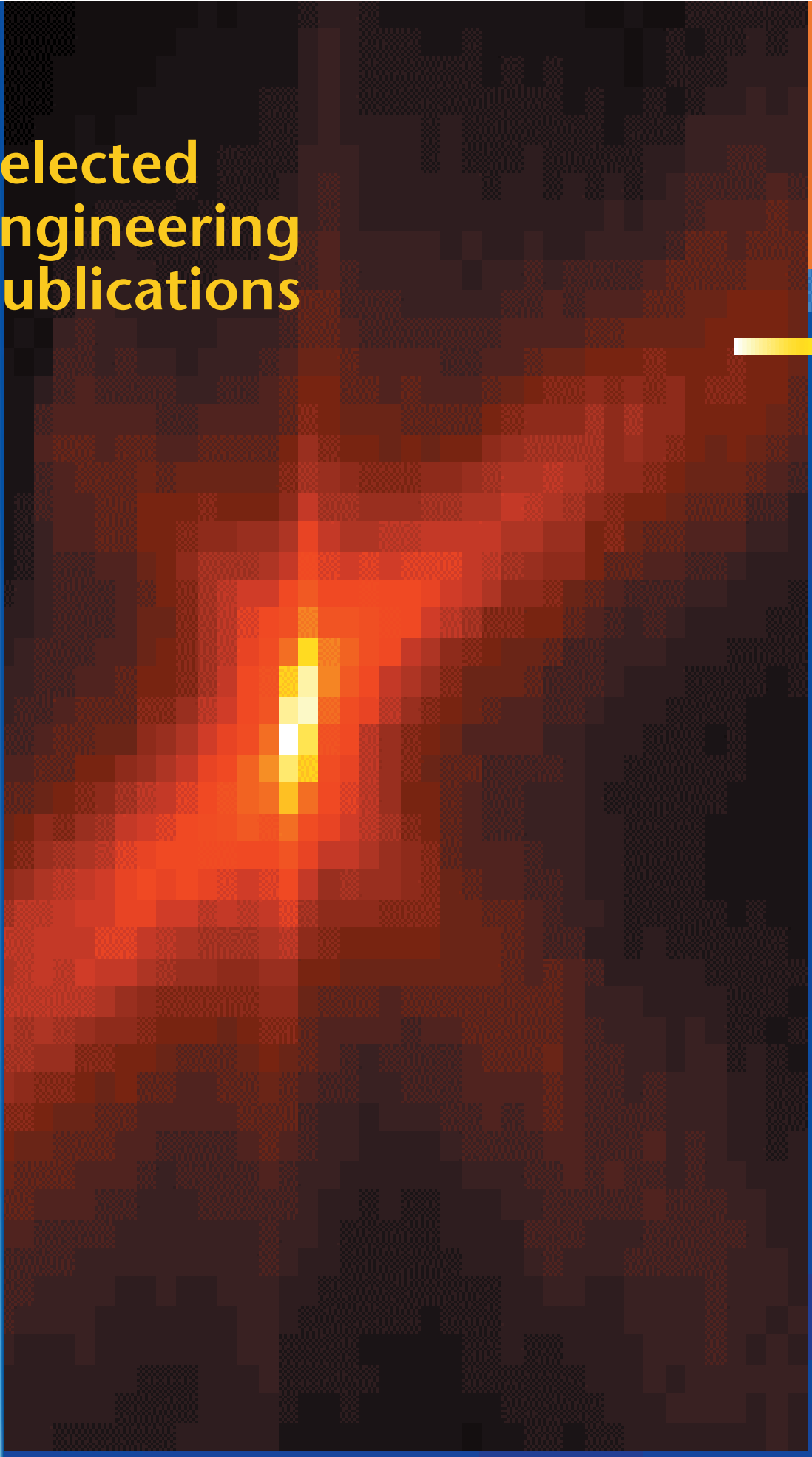

Berryman, J., L. Barcka, and G. Papanicolaou (2000), "Time reversal acoustics for multiple targets," *J. Acoust. Soc. Amer.* (UCRL-140465).

Buettner, H. M., W. Labiak, and A. Spiridon (2000), "Remote instrumentation and safeguards monitoring for the Star project," Nuclear Plant Instrumentation, Control and Human-Machine Interface Technologies Meeting, American Nuclear Society, Nov. 13–16.

Buettner, H. M., E. Didwall, F. Followill, D. McCallen, and R. Morey (2000), "GPR characterization of underground facilities at NTS," *Proc. of the Unattended MASINT Sensor and Geophysical Conf.,* Quantico, Virginia, Nov. 7–8.

Burke, G. J., and D. J. Steich (2000), "Numerical modeling of shielding by a wire mesh box," 16th Annual Review of Progress in *Applied Computational Electromagnetics*, pp. 452–459, Monterey, California, March 20–24.

Candy, J., and D. Chambers (2000), "The role of the time reversal processor in acoustic signal processing," *J. Acoust. Soc. Amer.* (UCRL-JC-141160).

Candy, J., D. Chambers, R. Huber, and G. Thomas (1999), "Matched-field imaging of laser generated ultrasound for nondestructive evaluation," *J. Acoust. Soc. Amer.* (UCRL-133397).

Candy, J., D. Chambers, R. Huber, and G. Thomas (2000), "Ultrasonic matched-field imaging for nondestructive evaluation," Ocean Imaging Conf. (UCRL-136369).

Candy, J., (2000), "The role of the time reversal in signal processing," C.A.S.I.S. Workshop at LLNL (UCRL-VG-141331).

Caporaso, G., and J. McCarrick (2000), "Ion-Hose instability in long pulse induction accelerators," *Proc. of the 20th Int. LINAC Conf.,* pp. 500–02, Monterey, California, Aug. 21–25.

Chambers, D., and A. Gautesen (2000), "Multiple eigenvalues of the time reversal operator for a single hard scatterer," *J. Acoust. Soc. Amer.* (UCRL-139914).

Chambers, D., and A. Gautesen (2000), "Time reversal for a single spherical scatterer," *J. Acoust. Soc. Amer.* (UCRL-JC-141165).

Chen, Y.-J., D. Ho, J. McCarrick, A. C. Paul, B. Poole, S. Sampayan, L. Wang, and J. Weir (2000), "Physics design of the ETA-II/Snowtron double pulse target experiments," *Proc. of the 20th Int. LINAC Conf.,* pp. 482–4, Monterey, California, Aug. 21–25.

Conrad, D. C. (2000), "Underground explosions are music to their ears," *Science and Technology Review,* pp. 4–11, July/Aug. (UCRL-52000-00-7/8).

Conrad, D. C., P. Egan, and the LLNL/BN SCE Team (2000), presented by Ray Heinle, "U1a vessel experiments: OBOE and beyond," JOWOG 32 PDT, Aldermaston, England, Nov 29–Dec. 1.

Cooperstein, G., W. DeHope, *et al*. (2000), "Progress in rod pinch electron beam diodes as intense x-ray radiographic sources," 13th Int. Conf. on High-Power Particle Beams (BEAMS 2000), Nagaoka, Japan, Jun. 25–30.

Cunningham, C. T., and R. S. Roberts (2001), "An adaptive path planning algorithm for cooperating unmanned air vehicles," *Proc. of the IEEE Int. Conf. on Robotics and Automation*, Seoul, Korea, May (UCRL-JC-140415).

Dudley, D. G., H.-Y. Pao, and D. A. Hill (2000), "Introduction to special issue," *IEEE Transactions on Antenna and Propagations*, **48**, No. 9, Sept.

Eppler, W. G., D. W. Paglieroni, M. Petersen, and M. J. Louie (2000), "Fast normalized cross-correlation of complex gradients for autoregistration of multi-source imagery," ASPRS DC 2000 Conf., May 22–27.

Falabella, S., Y.-J. Chen, T. Houck, J. McCarrick, S. Sampayan, and J. Weir (2000), "Effect of backscattered electrons on electron beam focus," *Proc. of the 20th Int. LINAC Conf.*, pp. 458–60, Monterey, California, Aug. 21–25.

Ge, J., D. Ciarlo, P. Kuzmenko, B. Macintosh, C. Alcock, and K. Cook (2000), "Etched silicon gratings for NGST," *Next Generation Space Telescope Science and Technology*, ASP Conf. Series, **207**, p. 457.

Ge, J., D. Ciarlo, P. Kuzmenko, C. Alcock, B. Macintosh, R. Angel, N. Woolf, M. Lloyd-Hart, R. Q. Fugate, and J. Najita (2000), "Adaptive optics high resolution spectroscopy: present status and future direction," *Proc. Imaging the Universe in Three Dimensions,* ASP Conf., **195**, p. 568.

Ge, J., J. P. Lloyd, D. Gavel, B. Macintosh, C. E. Max, D. Ciarlo, P. Kuzmenko, and J. R. Graham (2000), "High spectral and spatial resolution spectroscopy of YSOs with a silicon prism and adaptive optics," BAAS, **197**, p. 5201.

Guethlein, G., T. Houck, J. McCarrick, and S. Sampayan (2000), "Faraday cup measurements of ions backstreaming into an electron beam impinging on a plasma plume," *Proc. of the 20th Int. LINAC Conf.,* pp.467–9, Monterey, California, Aug. 21–25.

Handler, F. A., and L. C. Ng (2000), "Signal detection and feature extraction for target/decoy discrimination from IFT-1A flight experimental data: a technical response to Dr. Ted Postal's allegations (U)," published as a POET document.

Holzrichter, J. F., and L. C. Ng (2000), "Speech articulator and user gesture measurements using micropower, interferometric EM-sensors," IEEE-Instrumentation and Measurement Technology Conf. (IMTC), Budapest, Hungary, May 21–23 (UCRL-JC-140496).

Huber, R., J. Candy, D. Chambers, and G. Thomas (1999), "Processing of laser-based ultrasound for matched-field imaging," Quantitative NDE Conf. (UCRL-134055).

Le Sage, G. P., S. G. Anderson, T. E. Cowan, J. K. Crane, T. Ditmire, and J. B. Rosenzweig (2000), "RF photoinjector development for a short-pulse, hard x-ray Thomson scattering source," AIP Conf. Proc. for the Advanced Accelerator Conf., Santa Fe, New Mexico, (UCRL-JC-140148).

McCarrick, J. (2000), "The effect of asymmetric plasma plumes on the transport of high-current electron beams," *Proc. of the 20th Int. LINAC Conf*, pp. 461–3, Monterey, California, Aug. 21–25.

Merrill, R. D., *et al.* (2001), "Material transfer system in support of the plutonium immobilization program," *Proc. of the American Nuclear Society Ninth Topical Int. Meeting on Robotics and Remote Systems*, Seattle, Washington, March 4–8.

Merrill, R. D., *et al.*, (2001), "Remote equipment development for the plutonium ceramification test facility at LLNL," *Proc. of the American Nuclear Society Ninth Topical Int. Meeting on Robotics and Remote Systems*, Seattle, Washington, March 4–8.

Ng, L. C., G. C. Burnett, J. F. Holzrichter, and T. J. Gable (2000), "Denoising of human speech using combined acoustic and EM sensor signal processing," IEEE ICASSP-2000, Istanbul, Turkey, Jun. 6 (UCRL-JC-136631).

Paglieroni, D. W., and R. S. Roberts (2000), "Optimal segmentation strategy for compact representation of hyperspectral image cubes," *Proc. ASPRS DC 2000 Conf.*, May 22–27.

Pao, H.-Y. (2000), "In memoriam of James R. Wait," Guest Editor, *IEEE Transactions on Antenna and Propagations*, Special Issue, **48**, No. 9, Sept.

Pao, H.-Y., and J. R. Wait (2000), "Electromagnetic induction and surface impedance in a half-space from an overhead moving current system, *IEEE Transactions on Antenna and Propagations*, **48**, No. 9, Sept.

Poole, B. R., Y. J. Chen, A. C. Paul, and L.-F. Wang (2000), "Particle simulation of DARHT-II downstream transport," *Proc. of the 20th Int. LINAC Conf*, Monterey, California, August 21–25.

Puso, M. A., and T. A. Laursen (2000), "A method for 3D contact surface smoothing," *Int. J. for Numerical Methods*.

Puso, M. A. (2000), "An energy and momentum conserving algorithm for rigid-flexible body dynamics," *Int. J. for Numerical Methods*.

Richardson, R., S. Sampayan, and J. Wier (2000), "Elliptical x-ray spot measurement," *Proc. of the 20th Int. LINAC Conf.*, Monterey, California, August 21–25.

Roberts, R. S. (2000), "Characterization of hyperspectral data using a genetic algorithm, IEEE Thirty-Fourth Asilomar Conf. on Signal, Systems and Computers, Pacific Grove, California, Oct. 29–Nov. 1.

Sampayan, S., G. Caporaso, Y.-J. Chen, S. Falabella, D. Ho, T. Houck, E. Lauer, J. McCarrick, R. Richardson, D. Sanders, and J. Weir (2000), "Beam-target interaction experiments for Bremsstrahlung convertor applications," *Proc. of the 20th Int. LINAC Conf.*, pp. 464–6, Monterey, California, Aug. 21–25.

Tomascik-Cheeseman, L. M., R. Raja, L. M. Kegelmeyer, S. L. Mabery, B. J. Marsh, F. Marchetti, J. Nath, and A. J.Wyrobek (2000), "Parallel expression analyses of DNA repair genes in adult mouse tissues using cDNA microarrays," *Proc. of the Environmental Mutagen Society*, New Orleans, Louisiana, in *Environmental and Molecular Mutagenesis*, **35**, No. 31, p. 61, April.

Wang, L., G. J. Caporaso, and E. G. Cook, "Modeling of an inductive adder kicker pulser for DARHT-2," *Proc. of the 20th Int. LINAC Conf.*, Monterey, California, August 21–25.

Wang, L., S. M. Lund, and B. R. Poole (2000), "Dipole septum magnet in the fast kicker system for multi-axis advanced radiography," *Proc. of the 20th Int. LINAC Conf.*, Monterey, California, August 21–25.

Author Index

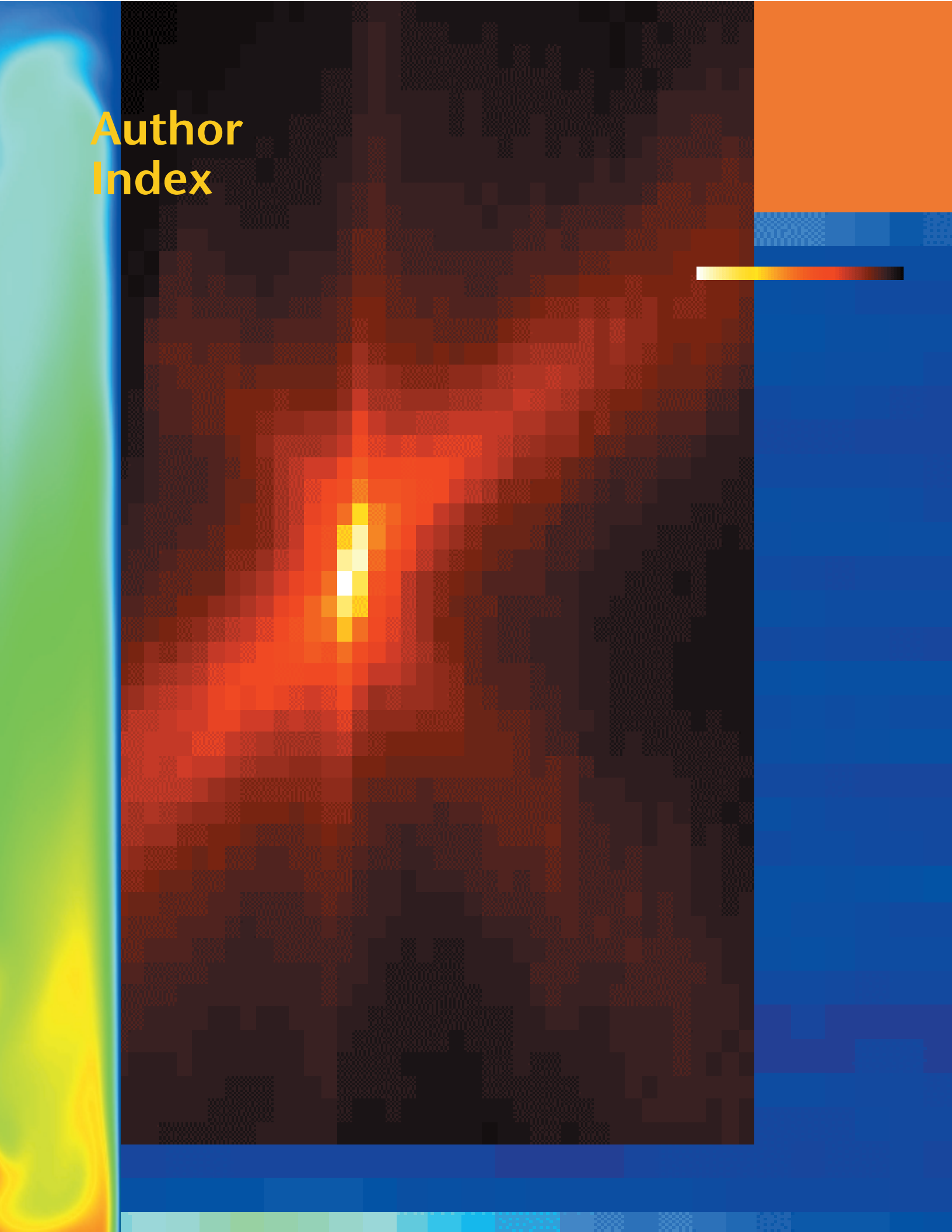

Anderson, G. . . . 3
Anderson, S. G. . . . 4
Aufderheide, III, M. B. . . . 9
Behymer, E. M. . . . 15
Bentereau, J. . . . 18
Birks, T. . . . 18
Bond, S. W. . . . 15
Bowers, M. . . . 18
Boyd, R. . . . 18
Candy, J. V. . . . 19
Champagne, N. J. . . . 5
Chinn, D. . . . 10
Clague, D. S. . . . 7
Coldren, C. W. . . . 14
Cooke, J. . . . 18
Cowan, T. E. . . . 3, 4
Crane, J. K. . . . 3, 4
Cross, R. . . . 3
Cunningham, C. T. . . . 13
Ditmire, T. . . . 3, 4
Goodman, D. M. . . . 9
Hall, J. M. . . . 9
Harris, J. S. . . . 14
Hays, G. . . . 3
Hilken, D. . . . 7, 17
Hills, R. . . . 13
Jackson, J. A. . . . 9
Jankowski, A. . . . 16
Kallman, J. S. . . . 6
Kecy, C. . . . 18
Kluiwstra, J.-U. . . . 17
Krulevitch, P. . . . 17
Kuo, P.-K. . . . 10
Larson, M. C. . . . 14
Leach, Jr., R. R. . . . 12
Le Sage, G. P. . . . 3, 4
Little, L. . . . 18
Logan, C. M. . . . 9
Martz, Jr., H. E. . . . 9
McCallen, D. B. . . . 12
Meyer, G. A. . . . 15
Miles, R. . . . 17
Moffitt, K. . . . 3
Morse, J. . . . 16
Ng, L. . . . 12
Patel, R. R. . . . 15
Petersen, H. E. . . . 14
Pocha, M. D. . . . 15
Puso, M. A. . . . 8
Roberts, R. S. . . . 13
Rosenzweig, J. B. . . . 4
Schach von Wittenau, A. . . . 9
Schumann, D. . . . 17
Seward, K. . . . 17
Sharpe, R. M. . . . 5
Shuttlesworth, R. . . . 3
Slone, D. M. . . . 9
Springer, P. . . . 3
Spruytte, S. G. . . . 14
Steich, D. J. . . . 6
Stephan, P. L. . . . 15
Stolz, C. . . . 10
Swift, D. . . . 11
Tsai, V. . . . 3
Wharton, K. . . . 3
Wheeler, E. K. . . . 7
White, D. A. . . . 5
Zywicz, E. . . . 8

Manuscript Date September 2001
Distribution Category UC-42

Work performed under the auspices of the U.S. Department of Energy by the University of California, Lawrence Livermore National Laboratory under Contract W–7405–Eng–48.
ENG-01-0004a-AD

Engineering Directorate
Lawrence Livermore National Laboratory
University of California
P.O. Box 808, L-124
Livermore, California 94551

http://www-eng.llnl.gov/